Master's thesis

NTNU
Norwegian University of Science and Technology

Hanne T. Nissen-Sollie

Study of Particle Sizes and Morphologies of Silica Coated Iron Oxide Nanoparticles Synthesized via a Semi-Batch Process

Master's thesis in Chemical Engineering
Supervisor: Sulalit Bandyopadhyay
Co-supervisor: Zeeshan Ali
June 2021

NTNU
Norwegian University of
Science and Technology

Hanne T. Nissen-Sollie

Study of Particle Sizes and Morphologies of Silica Coated Iron Oxide Nanoparticles Synthesized via a Semi-Batch Process

Master's thesis in Chemical Engineering
Supervisor: Sulalit Bandyopadhyay
Co-supervisor: Zeeshan Ali
June 2021

Norwegian University of Science and Technology

NTNU
Norwegian University of
Science and Technology

Abstract

Iron oxide nanoparticles (IONPs) have evoked much attention recently due to their outstanding properties, such as superparamagnetism and high surface-to-volume ratio. The particles find application in various fields, including biomedicine, catalysis, and water management. Their properties are strongly influenced by particle sizes, particle size distributions, and morphology. Rigorous criteria must be satisfied for various applications, and the development of different methods for tuning sizes is crucial.

The high surface tension of IONPs makes them prone to aggregation, which subsequently affects their physical and chemical properties. The use of stabilizing agents often solves this problem. However, in many cases, the functionalization of these particles is crucial to overcome such challenges. Silica coating of IONPs has become a promising and important approach in the development of magnetic nanoparticles since it improves their chemical stability in liquid and prevents aggregation. The silica shell provides a biocompatible and chemically friendly surface, enabling subsequent modification to optimize for application.

In this study, silanization of IONPs using a modified Stöber method in a semi-batch set up is investigated. This study supplements an earlier study performed by Ali [4], where a batch set up was used. The aim is to study the effects of introducing the reactants to the system over a period of time. It allows building up the molarities to control the nucleation and growth. The effect of different solvents, flow rates of TEOS and ammonium hydroxide, and masses of IONPs were investigated. Different combinations of parameters were carried out based on an experimental design created by the use of JMP. Highly stable particles, with sizes ranging from 737 ± 38 nm to 1058 ± 81 nm, have successfully been synthesized with various degrees of polydispersity. Four different morphologies were observed; spheres, incompletely fused particles, agglomerates, and irregular particles. The morphology appeared to be greatly dependent on the reaction parameters.

Magnetic measurements of the silica coated IONPs show that the particles possess superparamagnetic behavior, however, the magnetization is diminished at a higher degree than preferred as compared to the bare IONPs. Further studies will hence be vital to investigate how the iron content in the particles can be increased to fabricate particles with higher magnetization.

Sammendrag

Jernoksid nanopartikler har vekket mye oppmerksomhet den siste tiden på grunn av dere fremragende egenskaper som superparamagnetisme og høyt forhold mellom overflateareal og volum. Partiklene er anvendt i forskjellige fagfelt som for eksempel biomedisin, katalyse og vannbehandling. Egenskapene er svært avhengig av partikkelstørrelsen, partikkel -størrelsefordelingen og morfologien. Strenge krav stilles for at de skal kunne anvendes for ulike applikasjoner og det er derfor helt avgjørende å utvikle metoder for å kunne kontrollere størrelsene.

Jernoksid nanopartikler har høy overflatespenning, noe som gjør dem utsatt for aggregering, som videre påvirker de fysiske og kjemiske egenskapene. Funksjonalisering av partiklerne er derfor avgjørende for å overkomme slike utfordringer. Dekking av jernoksid nanoparticles med silisium har blitt en lovende og viktig tilnærming i utviklingen av magnetiske nanopartikler, siden det forbedrer deres kjemiske stabilitet i væske og forhindrer aggregering. Silisiumbelegget gir en biokompatibel og kjemisk vennlig overflate, som ytterligere mulig -gjør videre overflatemodifikasjon.

I dette studiet undersøkes silanisering av jernoksid nanopartikler ved hjelp av en modifisert Stöber-metode i et semi-batch-oppsett. Studiet supplerer til et tidligere studie utført med et batch-oppsett utført av Ali [4]. Et semi-batch oppsett brukes til å studere effekten av å introdusere reaktantene i systemet over en tidsperiode. Det gir muligheten for å bygge opp konsentrasjonene og kontrollere nukleering og partikkelvekst. Effekten av forskjellige løsningsmidler, strømningshastigheter av TEOS og ammoniumhydroksid og ulike masser av jernoksid nanopartikler ble undersøkt. Forskjellige kombinasjoner av parametere ble utført basert på et eksperimentelt design opprettet ved bruk av JMP. Stabile partikler, med størrelser fra 737 ± 38 nm til 1058 ± 81 nm, har blitt syntetisert med ulik grad av størrelsesfordeling. Fire forskjellige morfologier ble observert; kuler, ufullstendig smeltede partikler, agglomerater og uregelmessige partikler. Morfologien så ut til å være svært avhengig av reaksjonsparametrene.

Magnetiske målinger av silisiumdekkede jernoksid nanopartikler viser at partiklene har superparamagnetisk egenskaper, men magnetiseringen reduseres i høyere grad enn hva som er ønsket sammenlignet med udekkede jernoksid nanopartikler. Ytterligere studier vil derfor være avgjørende for å undersøke hvordan jerninnholdet i partiklene kan økes for å fremstille partikler med høyere magnetisering.

Preface

This thesis was written in the spring of 2021, as the final part of my MSc. in Chemical Engineering at the Norwegian University of Science and Technology.

I want to express my sincere gratitude to my supervisor, Assoc. Prof. Sulalit Bandyopadhyay, for his extraordinary support. His expertise and nurturing support was instrumental for this thesis. I would like to thank him for always being available and helpful.

Thanks also to Zeeshan Ali for being my co-supervisor and providing me with insightful suggestions and guidance throughout the process.

Thanks to everyone in the Particle Engineering Research Team for helpful inputs in the meetings.

Finally, I would like to thank my fellow students and friends at Chemical Engineering for making these five years unforgettable!

Declaration of Compliance

I, Hanne Nissen-Sollie, hereby declare that this is an independent work according to the exam regulations of the Norwegian University of Science and Technology (NTNU).
Signature:

Place and Date: Trondheim - Gløshaugen, June 2021

Table of Contents

List of Tables

List of Figures

Nomenclature

Acronyms

NPs	Nanoparticles
IONPs	Iron oxide NPs
cIONPs	Citrate coated IONPs
ScIONPs	Silica coated CIONPs
SEM	Scanning electron microscopy
S(T)EM	Scanning transmission electron microscopy
DLS	Dynamic light scattering
VSM	Vibrating Sample Magnetometer
PDI	Particle distribution index
TEOS	Tetraethyl orthosilicate
MQ	MilliQ

Symbol	***Definition***	***Unit***
T	Temperature	°C
t	Time	min
rpm	Revolutions per minute	r/min
F	Flowrate	mL/min

Chapter 1

Introduction

Nanotechnology is an advancing field that engages scientists worldwide with backgrounds in physics, chemistry, biology, and engineering. Nanotechnology includes dimensions ranging from sub nanometers to several hundred nanometers. What makes nanoparticles so unique is their extraordinary properties that deviate from their bulk properties and the possibility of tuning these properties to fit specified applications. Due to the small dimensions, nanomaterials have a high surface-to-volume ratio, and the number of surface atoms and ions is a significant factor. Different nanomaterials possess beneficial mechanical, chemical, optical, magnetic, and electrical properties. Today, extensive research is conducted, and the materials are already widely applied in the industrial sector. The properties of nanoparticles are not only due to the tiny sizes but also the degree of monodispersity, as they have a high degree of size dependency. For many purposed applications, obtaining monodisperse particles is desired. With a variation in size of less than 5%, nanoparticles possess higher performances as compared to corresponding polydisperse nanoparticles [24].

1.1 Motivation

Iron oxide nanoparticles (IONPs) are one of the most promising nanomaterials and are widely applied in catalysis [30], biomedicine [12], and water management [47] to mention a few. IONPs possess unique properties such as superparamagnetism, biocompatibility, and easy separation methodology [3]. There is a range of synthesis routes already developed for the fabrication of IONPs. One simple, efficient, frequently used, and well-established method is co-precipitation. However, there are some disadvantages to the method as well. The particles tend to give a broad size distribution and are prone to aggregation. In some cases, this problem is solved by the use of stabilizing agents. However,

in many cases, surface modification is needed to prepare them for application. Another big issue that needs to be taken into account, which also might be solved by surface modification, is that the particles need to fit into the surroundings where the application is intended. Different applications require different interactions between the surroundings and the nanoparticles. One way to make IONPs better suited for a wide range of applications is to coat them with silica. A layer of silica offers a biocompatible and chemically stable surface which hinders them from agglomeration and degradation. Silica is in addition relatively cheap and easily available. Silica coated IONPs find applications as oil tags [77], in electron therapy [26] or in COVID-19 test [68] recently developed at NTNU and emphasize the usefulness and relevance of the particles in the past, today, and probably for a long time to come.

There are already a few methods developed for the silanization of particles. However, there is a lack of clear understanding of the growth mechanism of the particles. More research on different synthesis routes is needed to better understand and manage the control of the size, size distribution, and morphology of these particles. This work aims to study the effect of using a semi-batch set up in a modified Stöber method for the silanization of IONPs. The reaction mediums will be introduced over time to investigate how the particle size and morphology might be influenced and find the parameters affecting the properties of silica nanoparticles.

1.2 Outline

This report consists of seven chapters, including this chapter. Chapter 2 explains the theoretical background, including the fundamentals of magnetic nanoparticles and crystallization. Chapter 3 and Chapter 4 present literature reviews on the synthesis of IONPs and silica coated IONPs, respectively. In Chapter 4, the materials and methods used in this study are presented. A brief overview of the characterization techniques is also covered in the same chapter. All results, followed by discussions, are covered in chapter 6. Finally, Chapter 7 contains the overall conclusions of the work and also includes suggestions for further work.

Chapter 2

Theoretical Background

In this chapter, fundamentals of magnetic particles, crystallization, and semi-batch processes are discussed to get a theoretical background of the concepts used in this study.

2.1 Magnetic Nanoparticles

Magnetic nanoparticles such as iron, cobalt, and nickel receive extensive attention due to their unique physical properties, making them convenient for various applications. Magnetic particles are used for data storage [101], in catalysis [30], and in biomedicine [12], to mention a few. These particles possess unique magnetic properties, such as superparamagnetism [6], which occur in single-domain nanoparticles. A magnetic field can be used to manipulate the particles, and the superparamagnetic property makes it easy to separate the particles from other mediums. However, magnetic particles are exposed to issues like rapid agglomeration, and oxidation [102], and surface modification is often essential for making them worthy for applications. Magnetite, Fe_3O_4, is probably the most popular magnetic nanomaterial due to better chemical stability and biocompatibility [45]. Magnetite is also the most magnetic material found naturally in nature [62].

2.1.1 Superparamagnetism

Superparamagnetism is a phenomenon where the magnetization in a material randomly flips direction under the influence of temperature. Superparamagnetism appears in sufficiently small ferromagnetic or ferrimagnetic nanoparticles. What sufficiently small nanoparticles mean is dependent on the material, but in general, when the diameter of the particle is below 2-30 nm [57]. Superparamagnets have a high density of magnetic domains, and

the spins are aligned parallel and move collectively [45]. In the absence of an external magnetic field, the average value of magnetization is zero. However, in the presence of a magnetic field, the particles get magnetized. This transition occurs below the Curie temperature of the material. For any ferromagnetic or ferrimagnetic material, this transition occurs above the Curie temperature. Figure 2.1 shows the magnetization of ferromagnetic, paramagnetic, and superparamagnetic materials as an effect of an applied magnetic field. As seen in the figure, superparamagnetic materials have combined properties of ferromagnetism and paramagnetism. The magnetization of a superparamagnetic material is zero when the magnetic field is zero. However, an external magnetic field will magnetize the particles. This behavior is similar to the behavior of paramagnets, however, as the figure suggests, the magnetic susceptibility of superparamagnets is much greater than that of paramagnets. On the other hand, the magnetization of a ferromagnet is remnant in the absence of a magnetic field, as illustrated in the figure.

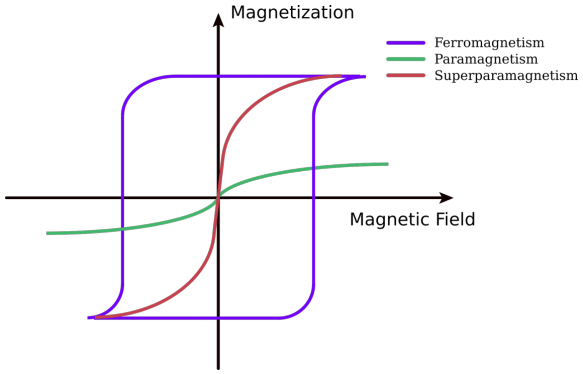

Figure 2.1: The magnetization as a function of magnetic field for ferromagnetic, paramagnetic and superparamagnetic materials [64].

2.1.2 Reduction, Nucleation and Growth of Metal Nanoparticles

Several different methods for the preparation of metal nanoparticles are developed. These methods are categorized as bottom-up, or top-down approaches [39]. The top-down approach starts with larger dimensions and breaks down the structure of a substance, while the bottom-up approach builds up the desired product layer by layer. To synthesis metallic nanoparticles, the reduction of metallic precursors is one of the most commonly used methods. That is a bottom-up approach, where in an appropriate medium, ionic salts are reduced in the presence of a surfactant and a reducing [32]. Reduction of the salts are used to prepare supersaturated solutions of metallic solids, and the concentration can easily be controlled.

The pathway for synthesizing stable nanoparticles from a metal precursor consists of three steps [96]. The first step is the reduction of the precursor, which is described by the following equation:

$$\mathrm{aM}^{n+} + \mathrm{bR} \longrightarrow \mathrm{aM}^{0} + \mathrm{bO} \tag{2.1}$$

where M is the metallic precursor, R is the reducing agent, and O is the oxidized compound, a and b are stoichiometric coefficients. The metal atoms gather in clusters following:

$$\mathrm{xM}^{0} \leftrightarrow (\mathrm{M}^{0}_{x})_{\mathrm{cs}} \tag{2.2}$$

where cs marks the critical size and x is a stoichiometric coefficient. When they obtain a critical size where they are stable, they start separating as nuclei described by the following equation:

$$(\mathrm{M}^{0}_{x})_{\mathrm{cs}} + \mathrm{yM}^{0} \leftrightarrow (\mathrm{M}^{0}_{x+y})_{n} \tag{2.3}$$

The next step is growth which is the addition of metal atoms onto particles having a high free surface energy:

$$(\mathrm{M}^{0}_{x+y})_{n} + \mathrm{mM}^{0} \longrightarrow \mathrm{M}^{0}_{n+m} \tag{2.4}$$

These further grow by diffusion or aggregation to produce stable nanoparticles:

$$\mathrm{M}^{0}_{n+m} + \mathrm{nM}^{0} \longrightarrow \mathrm{M}^{0}_{\star} \tag{2.5}$$

where $M^{0}_{\star}$ is a stable nanoparticle. The size of the particle is dependent on the supersaturation, the fraction of solute relative to the amount of metal in the nucleation, and the degree of aggregation [11]. To synthesis and control the properties of magnetic nanoparticles, understanding crystallization and supersaturation are essential.

2.2 Crystallization

Crystallization is a physical transformation of a liquid, solution, or gas into a crystal. A crystal is a solid characterized by an ordered internal arrangement of building units. When crystallization occurs, matter undergoes a phase transition from high free energy, disordered state, to a low free energy state [63]. Crystallization can be seen as a two-step process; the first is nucleation, followed by crystal growth. Understanding and separating the nucleation and growth regions of particles during synthesis is the key to obtain uniform particles.

2.2.1 Supersaturation

Supersaturation is the ability of a system to precipitate. A state of supersaturation is required for crystallization to occur. When a system is supersaturated, it possesses excess

free energy, and it is in a non-equilibrium state, allowing a solid phase to appear in the solution. When crystallization occurs, the free energy in the system consequently decreases. Supersaturation is defined as the ratio between the activity of a solute in an arbitrary state and the activity at equilibrium [11]:

$$S = \frac{a}{a*} \tag{2.6}$$

Where a is the activity and a* is the activity at equilibrium. Activity deviates from concentration by an activity coefficient factor. The activity coefficient factor is dependent on the ionic strength of the medium, charge, and size of each component. The activity is given by:

$$a = C\gamma \tag{2.7}$$

Where C is the concentration and γ is the activity coefficient. Concentration can substitute for the activity when dealing with dilute solutions. Supersaturation defined in terms of ionic product and solubility product can be expressed by:

$$S = \left(\frac{IAP}{K_{sp}}\right)^{\frac{1}{\nu}} \tag{2.8}$$

The driving force for crystallization is the difference between the chemical potential of a substance in a solution and the solid phase [63]:

$$\Delta\mu = \mu_1 - \mu_2 \tag{2.9}$$

The chemical potential is expressed by

$$\mu = \mu_0 + RTlna \tag{2.10}$$

Combining Equation 2.6, 2.9, and 2.10, the expression for the driving force in crystallization is:

$$\Delta\mu = RTln(S) \tag{2.11}$$

When S>1, the chemical potential is larger than zero, and the state of supersaturation is obtained. Spontaneous crystallization will occur.

Figure 2.2 shows the solubility and supersolubility curve for an arbitrary compound in solution [23]. As the temperature is increased, an increased amount of the substance dissolves in the medium. The arrow moving from point 1 to point 3 represents a cooling crystallization. At point 1, the medium is undersaturated, and no crystallization will occur. The system is stable as the concentration of dissolved solute is below the solubility curve. At point 2, the temperature is decreased, and the system crosses the solubility curve entering the metastable zone, and crystallization can occur. When the next curve is crossed at point 3, the solution enters the labile zone by a further decrease in the temperature. In the

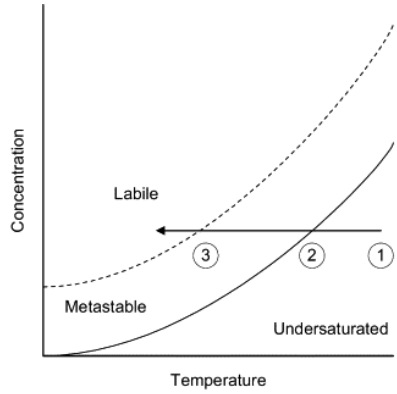

Figure 2.2: Concentration of a solid dissolving endothermically as a function of temperature [23].

labile zone, crystallization will occur spontaneously. Many crystallization processes, both industrial and laboratory, are carried out in the metastable zone, making it easier to control. The period between the initial moment of supersaturation and the appearance of the first nuclei, is defined as the induction time [10]. The induction time can vary from seconds to years. Crystallization would also occur having constant temperature but increasing the concentration to be higher than the solubility curve.

2.2.2 Classical Nucleation Theory

There are different nucleation processes. Figure 2.3 shows an overview of these processes [15]. Primary nucleation leads to new crystalline material, either by homogeneous or heterogeneous nucleation. Homogeneous nucleation occurs in the absence of any foreign surface, while heterogeneous nucleation happens on foreign surfaces. For secondary nucleation, particles of the solute induce the formation of new particles, i.e., also in the presence of a solid interface.

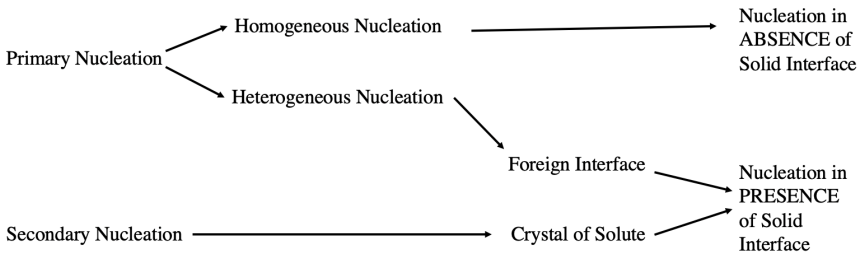

Figure 2.3: Overview of different nucleation processes. Reproduced from Beckmann [15].

Classical Nucleation Theory is a theoretical model and the most common theory to understand nucleation [40]. It was first established in 1926 by Volmer and Weber [98], and further developed by Becker and Döring [14] and Frenkel [27].

Figure 2.4 is a schematic representation of the change of free energy as a function of radius for homogeneous nucleation. It shows the nucleation barrier, ΔG_{nucl}, for a spherical nucleus. The red line, ΔG_{surf}, is the free energy change for the formation of a surface, the surface free energy. The blue line, ΔG_{vol}, is the change in free energy for phase transformation, the volume free energy. The total Gibbs free energy is the sum of these expressions and is represented by the green line:

$$\Delta G_{nucl} = \Delta G_{vol} + \Delta G_{surf} \tag{2.12}$$

For homogeneous nucleation of a spherical nucleus of radius r, the change in free energy is given by [40]:

$$\Delta G_{nucl} = \frac{-4\pi r^3}{3\nu} k_b T ln S + 4\pi r^2 \sigma \tag{2.13}$$

Where $4\pi r^3/3\nu$ is the number of molecules in a cluster of radius r, and ν is the volume per unit. k_b is the Boltzmann constant, T is the temperature, S is the supersaturation, and σ is the specific surface energy of the solid-liquid phase. As can be seen from 2.4, for a nucleus with a small radius, the creation of a new surface, ΔG_{surf}, is the dominating. For a nucleus of large radius, ΔG_{vol} is dominating. r_{crit} is the radius of a nucleus when the energy barrier is at its maximum and the probability of nucleus formation is at minimum. r_{crit} is found by differentiating Equation 2.13 with respect to r, and set the first derivative equal to zero, giving:

$$r_{crit} = \frac{2\sigma}{k_b T ln S} \tag{2.14}$$

The barrier for nucleation is then given by:

$$\Delta G_{nucl} = \frac{16\pi\sigma^3\nu^2}{3k_b^2 T^2 ln S^2} \tag{2.15}$$

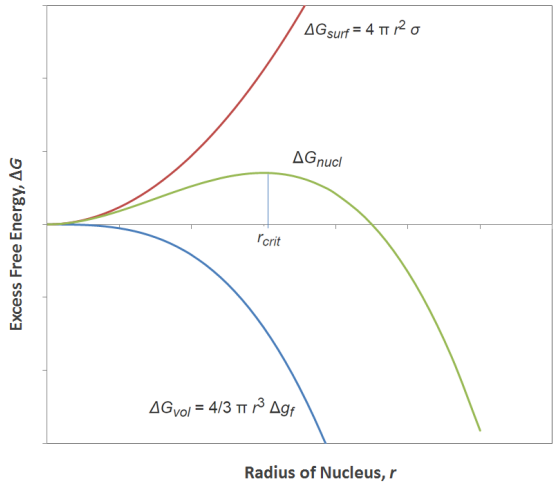

Figure 2.4: The change of free energy as a function of radius for a spherical nucleus [75].

The nucleation energy barrier can be used to express the nucleation rate, J. It is expressed in the form of the Arrhenius reaction rate equation:

$$J = Aexp\left[-\frac{\Delta G_{nucl}}{k_b T}\right] \tag{2.16}$$

where A is a factor determined by the reaction kinetics.

2.2.3 Growth

When a nucleus is formed, as the first step lowering the excess energy for a system in non-equilibrium, it is followed by size enlargement to minimize this free energy[44] further. Size enlargement is generally described by two processes, crystal growth, and agglomeration.

Crystal growth is the increase in the size of particles and leads to a crystal state. The final morphology and the size of a crystal are results of the enlargement process. Therefore, crystal growth is an important aspect to understand and be able to control the crystal properties and consequently to fabricate crystals suitable for different applications. The energy barrier for growth is lower than the barrier for nucleation [15].

Figure 2.5 illustrates the nucleation and growth stages in a crystallization process as the concentration, and consequently, the supersaturation changes over time. The LaMer diagram was proposed by LaMer and Dinegar in 1950 [48] and explains how monodisperse particles in a homogeneous solution are obtained. Nucleation occurs when the concentration reaches a level above the minimum nucleation concentration, C_{min}. The supersaturation is reduced after nucleation takes place as there are less solute available. When

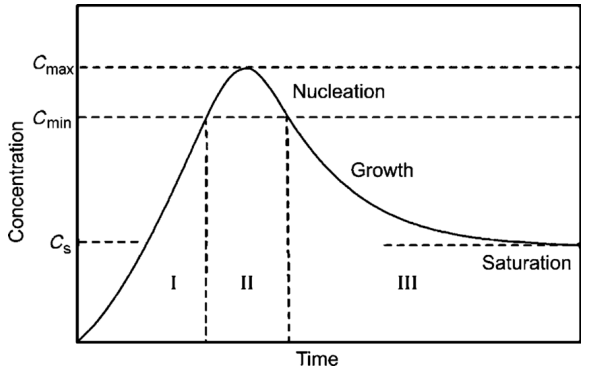

Figure 2.5: A LaMer diagram illustrating the stages of a crystallization process, (I) prenucleation, (II) nucleation and (III) growth [9].

the concentration is reduced below a certain value, and there is no addition of the solute, nucleation terminates, and only growth occurs. The nucleation should be rapid in order to obtain monodisperse particles [92].

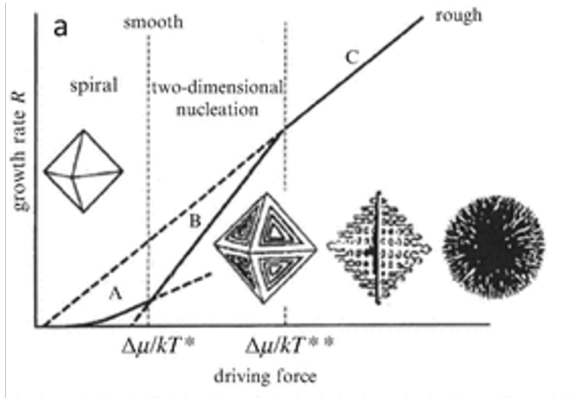

Figure 2.6: Growth rate as a function of driving force with corresponding growth mechanism and morphologies [5].

Crystal growth is a dynamic process where the attachment rate, J_{on}, of monomeric units, which are either atoms, ions, or molecules, exceeds the detachment rate. J_{off} [73]. The following equation can express the rate:

$$R = \alpha(J_{on} - J_{off}) \tag{2.17}$$

When $R = 0$ at $J_{on} = J_{off}$, the system is in equilibrium. The attachment rate, J_{on}, is dependent on the solute concentration in the medium, and the detachment rate, J_{off}, is determined by the bonding strength for neighbor monomer units [11]. This strength is mainly dependent on the temperature, making both supersaturation and temperature important parameters for crystal growth.

Crystal growth consists of two processes. Diffusion of growth units from solution to the crystal surface and surface reactions that result in attachment of the growth units [66]. These processes are referred to as diffusion- and reaction-controlled mechanisms. The overall growth rate can be expressed by:

$$G_r = k_g(S-1)^g \tag{2.18}$$

where k_g is the growth constant, which is solubility- and temperature-dependent, S is the activity-based supersaturation, and g is the growth order. The growth order reveals the growth mechanism. Figure 2.6 shows the growth rate as a function of driving force for a given crystal. Three crystal growth mechanisms are illustrated in the figure with the respective morphology. Spiral growth is a result of lower supersaturation, and the growth order is then $g = 2$. Two-dimensional nucleation growth is caused by low to moderate supersaturation, $g > 2$. At higher supersaturation, the surface roughness is increased, resulting in rough growth, $g = 1$. Rough growth is diffusion-controlled, while spiral- and two-dimensional growth are reaction-controlled. At even higher supersaturation, non-crystallographic branching, and formation of polycrystalline, typical spherical structures, can result from interface instability.

Agglomeration is a phenomenon occurring when two particles physically collide, and the attractive forces between the particles exceed the repulsive forces for the particles to disintegrate [15]. Repulsive forces, such as electrostatic, can hinder agglomeration. The agglomeration tendency depends on the surface charge of the particles, often referred to as the zeta potential. A low zeta potential will often result in agglomeration, while a higher zeta potential often hinders particle contact. Agglomeration can also be avoided by additives such as surfactants. Different mechanisms may lead to agglomeration; it may be a result of random Brownian motion or by the influence of gravity, among others [87].

Chapter 3

Iron Oxide Nanoparticles

Iron and oxygen can chemically bond to form plenty of different combinations. Today 16 different combinations are identified. Among these, magnetite (Fe_3O_4), maghemite (γ-Fe_2O_3) and hematite (α-Fe_2O_3) are the most common combinations found naturally on earth [3].

Iron oxide nanoparticles (IONPs) possess unique magnetic properties. The particles exhibit higher chemical stability than similar magnetic nanoparticles and are also biocompatible, making them excellent candidates for biomedical applications. The superparamagnetic behavior makes the separation methodology easy. The particles are widely applied today; examples are as a contrast agent in magnetic resonance imaging [76], in drug delivery [20], and in water management [47], to mention a few.

Different applications of IONPs require different morphology, size, and size distribution. Knowledge of how to obtain reasonable control of the product is hence necessary. Control of the supersaturation, the nucleation step, and the growth process are essential to tune the properties to meet the criteria for different applications.

3.1 Synthesis of Iron Oxide Nanoparticles

Today, several synthesis routes for the fabrication of iron oxide nanoparticles are developed. Co-precipitation [71], thermal decomposition [85], microemulsion [69] are examples of different routes using chemical techniques. There are also physical methods, for example, the use of aerosol technique [94], and biological methods, for example, synthesis mediated by proteins [41]. However, chemical techniques are of more interest due to low production cost, and high yield [3]. There are advantages and disadvantages for all the synthesis routes. Different methods offer different sizes, shapes, and morphologies. Some

methods are performed at room temperature, while others require elevated temperatures. To prepare IONPs for a specific application, one needs to consider the pros and cons of the different routes. In Table 3.1 a selection of some chemical techniques is listed with their advantages and disadvantages. In this work, co-precipitation is used to synthesize IONPs and will therefore be discussed in detail in the following section.

Table 3.1: Chemical techniques for preparation of IONPs [3, 102].

Method	Advantages	Disadvantages
Co-precipitation	Simple, effective	Broad size distribution, poor crystallinity, aggregation
Thermal decomposition	High yield, control of size and shape	High temperature required
Microemulsion	Control of particle size, homogeneous	Big volumes of solvent, poor yield, time

3.1.1 Co-precipitation

Co-precipitation is one of the most used and well-known synthesis routes for the production of IONPs. It was reported by Mossart et al. [59] in 1981. The method is efficient and straightforward; however, broad size distribution and poor crystallinity are often achieved. Aggregation of the particles is also a faced problem, affecting the final size and morphology. The particles are formed under high supersaturation resulting in a considerable amount of particles.

In a typical synthesis, as reported by Puddu et al. [77], iron salts, $FeCl_3{\cdot}6\,H_2O$ and $FeCl_2{\cdot}4\,H_2O$ in a ratio 2:1, are used as iron precursors in a basic solution. A basic solution is achieved by the addition of base either by fast addition or slow addition over time [46]. Different bases such as NH_4OH, KOH or NaOH [58] might be used. As soon as the base is added, the reaction mixture, which originally is orange, immediately turns black [99]. The overall chemical reaction taking place in co-precipitation is represented by:

$$Fe^{2+} + 2\,Fe^{3+} + 8\,OH^- \rightarrow Fe_3O_4 + 4\,H_2O \tag{3.1}$$

In the co-precipitation process, two separate steps are involved, the nucleation and the growth [19]. The nucleation takes place when the concentration of the involved species reaches a critical value. The nucleation is followed by slow growth by the diffusion of solutes. The nucleation and growth should be separated to achieve monodisperse particles, meaning burst nucleation should be accomplished, and the nucleation should terminate before the growth stage begins [95]. This is demonstrated by the LaMer diagram as described in Section 2.2.3. Several parameters may be varied in the co-precipitation method,

including the temperature, the stirring rate, pH, and if the synthesis is performed under a non-oxidizing atmosphere or not.

A non-oxidizing atmosphere can be obtained by bubbling nitrogen gas through the reaction mixture. When nitrogen is used, studies show that the obtained sizes are smaller than compared to using natural atmosphere, i.e., in the presence of oxygen [88]. This protects the IONPs from oxidation. In order to avoid magnetite oxidizing into ferric hydroxide, γ-Fe_2O_3, it is essential to leave the reaction mixture free from oxygen.

Ramadan et al. [81] studied the effect of different values of pH on the particle sizes obtained by using co-precipitation. They used pH varying from 8 to 12.5 resulting in particle sizes varying from 10 to 13 nm with a minimum reached at pH 9.5. They also report that the pH has a significant influence on the resulting phases. Magnetite was formed at all pH values; however, with increasing pH, the contribution of goethite was significant. Sun et al. [93] report that the particle sizes decreased up to a particular pH value, then the sizes increased with further increasing of the pH. In other words, they observed the same trend as Ramadan et al.. However, they report that the smallest sizes were obtained at pH 11. A more detailed reaction mechanism for the co-precipitation was proposed by Lian et al. [50] to describe the effect of pH:

$$\mathrm{Fe^{3+}} + 3\,\mathrm{OH^-} \rightarrow \mathrm{Fe(OH)_3} \tag{3.2}$$

$$\mathrm{Fe(OH)_3} \rightarrow \mathrm{FeOOH} + \mathrm{H_2O} \tag{3.3}$$

$$\mathrm{Fe^{2+}} + 2\,\mathrm{OH^-} \rightarrow \mathrm{Fe(OH)_2} \tag{3.4}$$

$$\mathrm{FeOOH} + \mathrm{Fe(OH)_2} \rightarrow \mathrm{Fe_3O_4} + 2\,\mathrm{H_2O} \tag{3.5}$$

Fe^{3+} ions react with hydroxyl ions produced as a result of base addition, i.e., by increasing the pH of the solution. $Fe(OH)_3$ precipitates first as the solubility product of $Fe(OH)_3$ is smaller than of $Fe(OH)_2$. $Fe(OH)_3$ is then transferred into goethite, leaving a water molecule. When more hydroxyl ions are produced, $Fe(OH)_2$ will reach its solubility product which in order will grow on the already formed FeOOH nuclei, and the product will be uniform magnetite [50]. With these reactions in mind and the observed sizes, Sun et al. [93] suggested that nucleation of IONPs is more likely to happen at pH below 11, while growth is more likely to happen at pH higher than 11.

By using different temperatures in co-precipitation, the sizes of the resulting IONPs may be tuned. Mahdavi et al. [56] reported that the sizes decrease with the increase in temperature up to 45 °C, where a minimum is reached. When the temperature is further increased, the sizes increase following the temperature, and a higher degree of polydispersity is also reported. By increasing the temperature, the degree of aggregation of the nucleus is brought down; however, when the temperature reaches a certain level, in this

case, 45°C, growth is more likely to happen resulting in bigger particles. It is also suggested that with a higher temperature and thus higher overall energy in the system, there is a rise in particles' collisions. Another explanation of the size increase of particles at higher temperatures is suggested by Bhattacharya et al. [16], the total volume of the solution increases with increasing temperature resulting in a lowered supersaturation which hinders burst nucleation. There are also studies claiming that synthesis temperature varying from 20 °C up to 50 °C have little or no influence on the particles [8].

The stirring rate affects the nucleation and growth of particles which in turn affects the final particle size. Mahdavi et al. [56] studied the effect of stirring rate for particle sizes obtained by co-precipitation. They report that by increasing the stirring rate from 400 to 800 rpm, the particle sizes decrease due to increased energy transferred to the mixture, making the solution dispersed into smaller droplets. Another explanation of the reduction in particle sizes is suggested by Hua et al. [37]. It is that due to a higher degree of agitation, the growth kinetics is reduced. Mahdavi et al. [56] also demonstrated that a too high stirring rate leads to the generation of bubbles in the solution and thus leading to a higher probability of oxidation. When a lower stirring rate is used, the nucleating species are not equally dispersed in solution and tend to aggregate, explaining the bigger sizes obtained.

3.2 Surface Modification of Iron Oxide Nanoparticles

As mentioned before, IONPs synthesized by co-precipitation are prone to aggregation due to great surface area to volume ratio, thus high surface energy. Surface engineering is often needed to make the particles stable and apt for applications. Functionalization of IONPs can conquer such barriers. The main motives of functionalization are; to enhance or change the dispersion, improve the surface activity, enhance the physicochemical and mechanical properties, and raise the biocompatibility [102].

IONPs may be functionalized using *in situ* or *post situ* approaches depending on the desired functionality. Examples of in situ functionalizations of IONPs are coating the IONPs with sodium oleate [93], oleic acid [33], or citrate [21] during the synthesis. These techniques are generally applied to alter the stability and properties of the IONPs. Post situ functionalization is, for example, the coating of the IONPs with a protective layer, for example, silica [53], for protection of the particles, but also to make the particle apt to the surroundings. Functionalization of IONPs with silica shells is described in detail in the next chapter. The IONPs used in this study are coated with citrate. The citrate coating of IONPs is described in the following section.

3.2.1 Citrate Coating of IONPs

Citric acid has been demonstrated to be a suitable candidate for the functionalization of IONPs to avoid their agglomeration. Citrate coating alters the repulsive interactions of

the particles, which, in order, gives thermodynamically stable solutions [21]. As it is a small molecule, it is not prone to the steric hindrance that large molecule surfactants and long polymer chains need to overcome [67]. IONPs coated with citric acid also exhibit hydrophilic properties. Citric acid has three carboxyl groups, whereas one or two are absorbed on the surface of the IONPs as suggested by Sahoo et al. [83]. Citrate coated IONPs may be achieved by introducing an aqueous solution of citric acid during co-precipitation as described by Nigam et al. [67]. Citric acid can then be directly attached to the surface of freshly prepared IONPs as illustrated by Rahimnia et al. [80] in Figure 3.1.

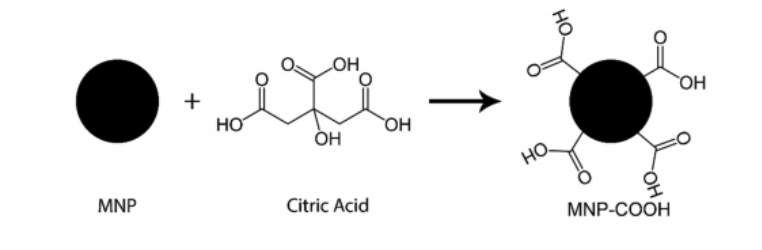

Figure 3.1: Mechanism of IONPs coated with citric acid illustarted by Rahimnia et al.[80] where MNP is an abbreviation for magnetic nanoparticle.

Chapter 4

Silica Coated Iron Oxide Nanoparticles

For many applications of IONPs, it is necessary to coat them in another material to prevent their agglomeration and degradation. Silica is widely used for this purpose as it is an ideal coating material. First of all, silica is cheap, and the silanization is performed under mild reaction conditions [52]. However, most importantly, the silica layer provides a biocompatible and chemically friendly surface for their use in biomedicine and bioengineering. A silica shell also protects the magnetic cores. The hydrophilic property of silica makes the particles well dispersed in the aqueous phase as the silica shell can screen magnetic dipole interactions. The silanol groups on the surface make surface modification easy, for example, for grafting of dye molecules on the surface [55].

4.1 Silanization

Due to the numerous benefits of silica coating, much research has been invested, and various methods have been developed for the silanization of particles. Aerosol pyrolysis [90] and microemulsion [51] are two examples.Another well-known method is the Stöber Method. The process is easy to operate, and cheap [82]. In this project, a modified Stöber method is used for the silanization process, and the technique is described in the following sections.

4.2 Stöber Method

The Stöber Method was initially reported by Stöber et al. [91] in 1968. The method is simple and well established, as great efforts have been dedicated to further studies of the method and the growth of silica particles. It is a sol-gel process where a silica precursor, typically tetraethylorthosilicate (TEOS), reacts with water in an alcoholic solvent using ammonia hydroxide as the catalyst.

There are two essential reactions taking place during the Stöber Method, hydrolysis and condensation. Hydrolysis can be seen as the reverse of condensation; it breaks down a compound by adding water, whereas condensation builds up by the removal of water [89]. The mechanism for the hydrolysis and condensation step in the Stöber Method is proposed by Han et al. [34]:

$$\mathrm{Si(OEt)_4 + xH_2O \leftrightarrow Si(OEt)_{4-x}(OH)_x + xEtOH} \tag{4.1}$$

$$\mathrm{2\,Si(OEt)_{4-x}(OH)_x \leftrightarrow (EtO)_{8-2x}(Si{-}O{-}Si)(OH)_{2x-2} + H_2O} \tag{4.2}$$

$$\mathrm{Si(OEt)_4 + Si(OEt)_{4-x}(OH)_x \leftrightarrow (EtO)_{7-x}\,(Si{-}O{-}Si)(OH)_{x-1} + EtOH} \tag{4.3}$$

The first step is the hydrolysis of TEOS to produce silanol monomers. The ethoxyl groups on TEOS are replaced by silanol groups. The two next steps represent growth. The silanol groups are combined by condensation with other silanol groups or react with unhydrolyzed or ethoxyl groups of TEOS. Branched siloxane clusters, which further grow into a silica network, are generated.

In literature, there are two different models proposed for the formation of colloidal silica particles, the monomer addition model and the controlled aggregation model [28]. The monomer addition model was developed by Matsoukas and Gulari in 1988 [60]. The model takes after the LaMer model described in Section 2.2.3, silica nuclei are formed through hydrolysis and condensation of TEOS, followed by growth by deposition of silanol monomers into primary particles and later to colloidal stable silica particles. A schematic of the model is shown in Figure 4.1. The model favors uniform, and monodisperse silica particles, which is justified by burst nucleation and uniform growth, typically achieved at high ammonia concentrations [34].

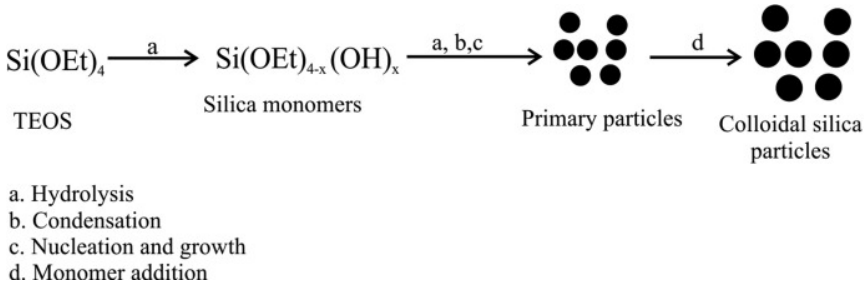

Figure 4.1: Monomer addition model [28] for the formation of silica particles.

The controlled aggregation model differs from the monomer addition model in that the nucleation occurs after condensation of monomers [18]. The nuclei are unstable and form small dense particles susceptible to aggregation until stability is obtained. Aggregation happens between different particle sizes and consequently causes polydisperse particles, typically achieved at lower ammonia concentrations [34]. A schematic of the controlled aggregation model is shown in Figure 4.2.

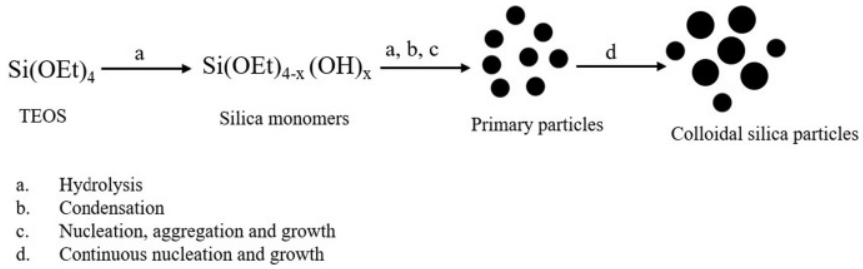

Figure 4.2: Controlled aggregation model [28] for the formation of silica particles.

4.2.1 Stöber Method for Silanization of Iron Oxide Nanoparticles

In the formation of the silica matrix, different compounds can get enclosed within the Si-O-Si bridges and encapsulated in silica as reported by Korzeniowska et al. [43]. A schematic of the process is shown in Figure 4.3. It is a commonly used method for the synthesis of IONPs encapsulated in silica. The method opens for the introduction of different compounds at different times. Some studies introduce the particles meant to be coated before the base, i.e., before the catalyst [77], while others like Lu et al. [53] propose to introduce the particles after the hydrolysis and condensation of TEOS have started and primary silica particles are produced.

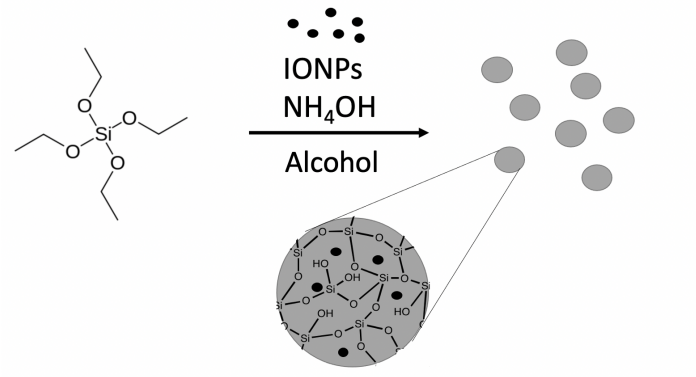

Figure 4.3: Encapsulation of iron oxide nanoparticles in silica shell. Reproduced and modified from the work of Korzeniowska et al. [43].

4.2.1.1 Effect of IONPs Mass

In the study performed by Lu et al. [53] different amounts of IONPs are added to the system to investigate the effect on the final particles. They claim that the concentration of IONPs can mediate the number of magnetic cores in the final coated particles added to the system. They reported that, by increasing the concentration of IONPs, the amount of IONPs in each particle increased, and less free silica was observed. At a low concentration of IONPs, there is an excess of silica to what is necessary to coat the IONPs. If the concentration of IONPs is high, the interactions between the magnetic particles are dominating, and the amount in each composite particle is increased. However, if the concentration exceeds a certain level, the result reveals non-spherical particles with a high degree of polydispersity [53]. A similar study performed by Pham et al. [72] contributes to these findings. They also report that at low IONPs concentration, free silica is observed, and at high concentration, irregular shaped particles are formed. Pham et al. also report that a lower concentration of IONPs reveals particles with bigger diameters meaning the silica shells are thicker.

4.2.1.2 Effect of Different Solvents

Different solvents in the Stöber method are a significant parameter, and various solvents are investigated and reported in the literature. The standard solvents are alcohols; however, there are examples where non-alcoholic solvents as toluene [49] and hexane [36] are introduced in addition as co-solvents. Different alcohols have various properties like polarity and viscosity. These properties are dependent on the structure of the alcohol, i.e., the chain length and the molecular weight. Alcohol with fewer carbon atoms is, in general, more polar than alcohols with longer carbon chains because the alcohol group is a higher

percentage of the entire molecule. Bari et al. [13] studied the effect of various alcohols on silica sizes. They found that the solvent properties greatly influence the hydrolysis and condensation rates of TEOS. If the polarity is the determining factor, alcohols with shorter chains should slow down the reaction rates as a polar solvent reduces catalytic activity by forming hydrogen bonds with hydroxide ions. On the other hand, if the molecular weight, and thus steric hindrance, is the determining factor, the reaction rates should be affected in the opposite direction, meaning shorter chain solvents give a faster reaction. Most studies published report that the reaction rates for different solvents are in random orders, and there are reasons to believe that the reaction rates can not be determined exclusively on these properties. Different authors, Harris at al. [35] and Mine et al. [61] among others, also report not only random order based on properties but also different orders compared to each other studies. Harris et al. [35]. According to the study performed by Bari et al., ethanol gives smaller particles than isopropanol. However, the polydispersity index is reported to be higher [13].

4.2.1.3 Effect of Ammonium Hydoxide Concentration

The concentration of ammonium hydroxide is a critical parameter for the synthesis of silica particles. Ammonium hydroxide is used as the catalyst to speed up the hydrolysis of TEOS. Han et al. [34] suggest that the concentration of ammonium hydroxide directly influences the hydrolysis and condensation rate in the reaction, which subsequently affects the particle sizes and size distribution. Their studies reveal that a low concentration of ammonium hydroxide results in small particles with a broad size distribution. A low concentration of ammonium hydroxide makes the hydrolysis rate of TEOS slower. Therefore, the nucleation is slow, which means that the growth of silanol groups starts while nucleation is still going on. As explained with the use of a LaMer diagram in section 2.2.3, rapid nucleation is the key to obtain monodisperse particles. When nucleation and growth are proceeding simultaneously, polydisperse particles are achieved.

4.2.1.4 Effect of TEOS Concentration

The ratio of TEOS may be varied. Van Helden et al. [97] investigated the effect of increasing the initial concentration of TEOS in the Stöber method. They report that an increment of the TEOS concentration results in a decrease in the particle sizes. However, the standard deviation increases and the particles become irregular shaped when the concentration is too high [97]. While Van Helden et al. reported a decrease in particle size with higher TEOS concentrations, other studies do not sympathize with these findings. Pham et al. [72] report that an increasing TEOS concentration gives a thicker silica shell of the coated particles. However, if the TEOS concentration is too high, free silica is observed as the thickness of the silica shells reaches a maximum. Bogush et al. [17] claim that elevated TEOS concentrations give bigger particle sizes with broader size distributions. If the ratio of TEOS to ammonia gets too high unreacted TEOS might be achieved.

4.2.1.5 Effect of Semi-Batch Set-up

Kim and Kim [42] studied the effect of using a semi-batch/batch method for hydrolysis of TEOS. TEOS in ethanol is fed into the reactor containing NH_4OH and ethanol at a constant feeding rate. They argue that a slow hydrolysis rate is achieved during the semi-batch process, giving larger particles with a narrow size distribution than a batch process. The authors claim a better control over the nucleation time and hydrolysis rate and hence the potential to tune the particle size, shape, and size distribution. In a semi-batch process, the reaction speed can be controlled as the reaction proceeds as reactants are added. As Kim and Kim increased the feed rate, the particle size in the semi-batch process decreased. The standard deviation also decreased until it reached a certain level and started increasing again. Luo et al. [54] also studied the effect of introducing a mixture of TEOS and ethanol into the reaction system, and their results match the findings of Kim and Kim. They report a decrease in the mean particle size with an increased TEOS feed rate. After TEOS is hydrolyzed, it may condense on existing nuclei or form new nuclei. If TEOS is added with a slow flow rate, growth is preferred, however with a higher rate of addition, the formation of new nuclei is favored due to excessive hydrolyzed TEOS [54]. A slow rate should hence be used when the preferred outcome is big particles.

Chapter 5

Methodology

Iron(II)chloride hexahydrate ($FeCl_2 \cdot 4\,H_2O$, $\geq$ 99%), sodium citrate dihydrate (Na-citrate, $\geq$ 99%) and tetraethyl orthosilicate (TEOS, reagent grade 98%) were purchased from Sigma-Aldrich® (Schnelldorf, Germany). Iron(III)chloride hexahydrate ($FeCl_3 \cdot 6\,H_2O$, $\geq$ 99%) were bought from Acros Organics (Geel, Belgium). Ammonium hydroxide solution (25 wt%), ethanol (96%) and 2-propanol (technical grade) were bought from Merck Life Sciences AS. All the chemicals were used as received without any further purification or modification. All solutions were prepared using distilled de-ionized water (MilliQ water), having a resistivity $\sim$18.2 MΩ/cm at 25°C, taken from Simplicity® Millipore (Darmstadt, Germany) water purification system.

5.1 Synthesis of Citrate Coated Iron Oxide Nanoparticles

Citrate coated iron oxide nanoparticles (cIONPs) were synthesized using a modified method as reported by Nigam et al. [67]. The protocol is described in detail in Appendix A.1. Briefly, 4.44 g of $FeCl_3 \cdot 6\,H_2O$ and 1.732 g of $FeCl_2 \cdot 4\,H_2O$ were dissolved in 80 mL MQ water in a three-necked jacketed reactor, connected to a Julabo water bath. The reactor was constantly flushed under a nitrogen atmosphere and mechanically stirred at 1000 rpm. The temperature of the water bath was raised to 70°C and maintained for 30 minutes. 20 mL of ammonia solution was added instantaneously, after which the temperature was maintained for another 30 minutes. 4 mL of citric acid aqueous solution (0.5 g/mL) was added to the reaction mixture. The temperature was slowly raised to 90°C and maintained for 60 minutes. The reaction mixture was cooled to room temperature and transferred to a centrifuge tube. The cIONPs were separated using a permanent magnet and cleaned with MQ water thrice. The set up is shown in Figure 5.1.

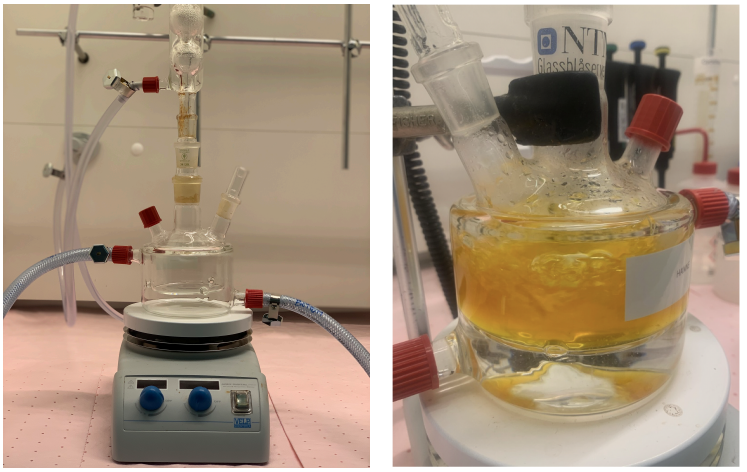

(a) **(b)**

Figure 5.1: Set up for the synthesis of cIONPs. **(a)** A three-necked jacketed reactor, connected to a Julabo water bath and a condenser. The condenser is connected to a slength line containing nitrogen gas. **(b)** Reaction medium before addition of ammonium hydroxide.

5.2 Silanization of cIONPs

The cIONPs, as synthesized in the previous section, were further coated with silica. The silanization process was carried out both as a batch process and a semi-batch process. The procedures are briefly explained in the following sections. Detailed protocols can be found in Appendix A.2 and A.3.

5.2.1 Batch Silanization of cIONPs

In a glass vial containing a magnetic stirrer bar, 19 mL solvent (ethanol or isopropanol) and 2 mL TEOS were added. The vial was placed on a stirrer plate with a stirring rate of 580 rpm. A calculated mass of cIONPs was cleaned thrice with the solvent and redispersed in 1 mL of the solvent. The cIONPs were separated between each cleanings using a permanent magnet for two minutes. The supernatant was discarded. The cIONPs were sonicated for 3 minutes, and pipette flushing was performed simultaneously for the last minute. After 15 minutes, the cIONPs were added to the vial, and the mixture was left for another 15 minutes to ensure complete mixing. A specific volume of NH_4OH was added. The reactions were carried out for 5 hours at room temperature. After 5 hours, the reaction mixture was transferred to a centrifuge tube using a disposable pipette. The silica coated cIONPs (ScIONPs) were cleaned several times with solvent and MQ water using a permanent magnet and finally redispersed in 25 mL MQ water.

5.2.2 Semi-Batch Silanization of IONPs

In a glass vial containing a magnetic stirrer bar, 18 mL solvent (ethanol or isopropanol) was added. The vial was placed on a stirrer plate with a stirring rate of 580 rpm. The cIONPs were cleaned according to the procedure described in the previous section and added to the glass vial. The mixture was lept for 15 minutes. A syringe was filled with a mixture of 2 mL TEOS and 1 mL solvent. A specific volume of NH_4OH was added to another syringe. The TEOS mixture and the NH_4OH were added to the glass vial using syringe pumps and tubes using different flow rates. The TEOS mixture was added for 60 min and 25 min. The NH_4OH was added for 60 min. The reactions were carried out at room temperature for 5 hours. The ScIONPs were cleaned as described in the previous section. A set-up is of the reaction is shown in Figure 5.2.

Figure 5.2: Set up for the synthesis of ScIONPs. A glass vial, used as reactor, placed on a stirring plate. The glass vial was equipped with a lid with holes, for the tubes connected to the syringes in the syringe pumps.

5.2.3 Experimental Design

A design of experiments was performed using JMP. JMP, developed by the JMP business unit of SAS Institute, is a series of computer programs for statistical analysis. A Custom Design platform, which constructs optimal design custom-built for an experimental setting [38], was used. Solvent, the mass of cIONPs, the flow rate of TEOS, and the flow rate of NH_4OH were used as parameters. The design of experiments is shown in Table 5.1. As will be seen later on in the result and discussion chapter, some additional experiments were performed.

For easier discussion in Chapter 6, the sample names in the following sections are based on the reaction parameters fixed in the specific experiment. The sample names consist of a letter followed by two numbers, and lastly, another letter. The first letter is either 'I' for isopropanol or 'E' for ethanol. The first number represents the mass of cIONPs in

milligrams, 25, 50, or 75. The second number represents the ammonium hydroxide flow rate and is either 0.1, 0.054, or 0.008. The last letter represents the flow rate of TEOS and is either 'L' for low flow rate, 0.03 mL/min, or 'H' for high flow rate, 0.08 mL/min. For example, for sample I-25*0.1-L, the reaction parameters would be as follows; isopropanol is used as the solvent, together with 25 mg cIONPs, an ammonium hydroxide flow rate of 0.1 mL/min, and TEOS flow rate of 0.3 mL/min.

Table 5.1: Custom design made in JMP.

	Solvent	Mass of cIONPs [mg]	TEOS [mL/min]	NH_4OH [mL/min]	Sample name
1	Isopropanol	25	0.03	0.1	I-25*0.1-L
2	Ethanol	75	0.08	0.008	E-75*0.008-H
3	Isopropanol	75	0.08	0.1	I-75*0.1-H
4	Isopropanol	25	0.08	0.008	I-25*0.008-H
5	Ethanol	50	0.03	0.054	E-50*0.054-L
6	Isopropanol	25	0.08	0.1	I-25*0.008
7	Ethanol	25	0.03	0.008	E-25*0.008-L
8	Isopropanol	75	0.03	0.008	I-75*0.008-L
9	Isopropanol	25	0.08	0.008	I-25*0.08-H
10	Isopropanol	75	0.03	0.008	I-75*0.008-L
11	Ethanol	25	0.08	0.1	E-25*0.1-H
12	Isopropanol	75	0.03	0.1	I-75*0.1-L
13	Ethanol	50	0.08	0.054	E-50*0.054-H
14	Ethanol	75	0.03	0.1	E-75*0.1-L

5.3 Characterization

Dynamic light scattering (DLS), scanning electron microscopy (SEM), scanning transmission electron microscopy (S(T)EM) with EDS, and vibrating sample magnetometer (VSM) were used for characterization of the cIONPs and ScIONPs. The working principle and sample preparation for the instruments are described in the following sections. The concentrations of the final products were also determined. The concentrations were found by taking 100 μl of the samples in three Eppendorf tubes and drying them in a vacuum oven at 65°C for 24 hours.

5.3.1 Dynamic Light Scattering

Dynamic light scattering (DLS) is used to determine hydrodynamic diameters of particles and particle size distribution dispersed in a liquid. A thin, electric dipole layer is present on the surface of a particle dispersed in a liquid. The size of the particle, including this layer, is referred to as the hydrodynamic size. Hydrodynamic sizes are hence bigger than sizes determined in the dry state. Brownian motion scatters laser light that is focused on the solution, and Stokes-Einstein equation is used for calculation of the hydrodynamic size of the particles [70]:

$$d_h = \frac{k_B T}{6\pi\eta D} \tag{5.1}$$

where k_B is the Boltzman constant, T is the absolute temperature, η is the solvent's viscosity, and D is the diffusion coefficient.

Hydrodynamic sizes were measured using a Malvern Zetasizer Nano-ZS instrument. This instrument can also measure the zeta potential, which is the charge that occurs in the electric dipole layer and reveals information about the stability of the particles in the liquid.

5.3.1.1 Sample Preparation

In a glass vial, 100 μL of a particular sample was diluted with 5.7 mL of MQ water. The diluted dispersion was sonicated for 2 minutes and filled into a folded capillary cell. The absorbance was set to 0.1. Both the hydrodynamic size and zeta potential were measured.

5.3.2 Scanning Electron Microscopy

Scanning electron microscopy (SEM) provides surface images of particles down to nanoscale by scanning the surface using a focused electron beam. SEM APREO manufactured by FEI and located at the cleanroom facilities at NTNU Nanolab was used. Detailed images providing information on the topography, morphology, composition, and crystalline structure are captured due to the great depth of focus. The images are generated by the interactions of electrons and the sample. The electrons are scattered, and detectors collect the signals [65].

5.3.2.1 Sample Preparation

A silicon wafer was cut into small squares and cleaned in a plasma chamber where organic and inorganic contaminants are removed from the surface, and radical sites are created. In an Eppendorf tube, 20 μL of sample in an aqueous solution was diluted with 980 μL MQ water. The diluted solution was dropped on the silicon wafer, and the water was

evaporated. The wafers were finally placed on copper conductive tape and placed in the chamber of the instrument.

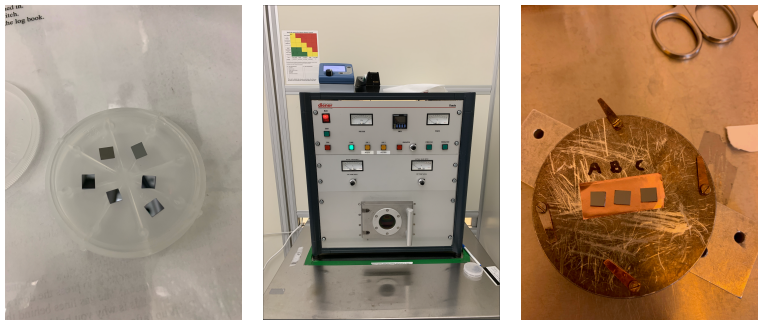

(a) **(b)** **(c)**

Figure 5.3: Stepwise preparation of the samples for use in SEM Apreo. **(a)** A silicon wafer cut in small squares, **(b)** the plasma cleaner used to clean the surface on the silicon wafers and **(c)** the silicon wafers, containing dry sample, placed on copper conductive tape on the sample holder.

5.3.3 Scanning Transmission Electron Microscopy (S(T)EM)

A Hitachi S-5500 S(T)EM located at the cleanroom facilities at NTNU Nanolab was used. S(T)EM has the same working principle as SEM. The difference is that S(T)EM can work in transmission mode as bright field and dark field detectors are installed. A Bruker EDX-system is also attached, allowing measurements of elemental mapping.

5.3.3.1 Sample Preparation

In an Eppendorf tube, 20 μL of the specific sample in an aqueous solution was diluted with 980 μL MQ water. The diluted solution was dropped on a copper grid, and the water evaporated. The grid was placed in a S(T)EM holder and placed inside the chamber.

5.3.4 Vibrating Sample Magnetometer

A vibrating sample magnetometer (VSM) is a magnetic measuring technique. A sample is vibrated perpendicularly to a uniform magnetizing field while the magnetic moment is measured. The technique uses Faraday's law of magnetic induction to obtain the magnetic moment [2].

$$\varepsilon = -N\frac{\Delta\Phi}{\Delta t} \tag{5.2}$$

where ε is the induced voltage, N is the number of loops, Φ is magnetic flux, and t is time.

5.3.4.1 Sample Preparation

The sample of interest was dried in a vacuum oven maintained at 65°C overnight. The dry sample was subsequently filled into a sample holder as shown in Figure 5.4.

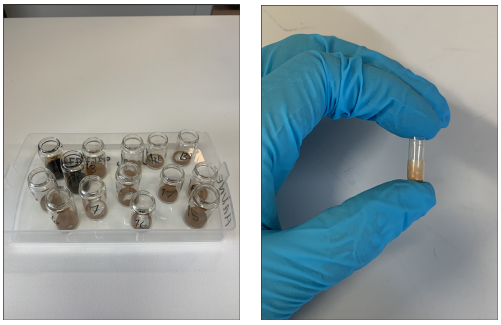

(a) **(b)**

Figure 5.4: Sample preparation for VSM measurements, **(a)** the samples were firstly dried in glass vials in a vacuum oven over night and **(b)** the powders were filled into a VSM sample holder.

Chapter 6

Results and Discussion

In this chapter, the results of the experiments conducted in this study are presented, including some discussion on the results and hypotheses. The first part contains the synthesis of citrate coated iron oxide nanoparticles (cIONPs), and the second part contains the silanization process of the already synthesized cIONPs. The second part is subsequently divided into two parts, first some initial studies to determine reaction parameters are presented, and secondly, the experimental design made in JMP. This last subpart also includes some extra experiments which were added to get a bigger picture.

Hydrodynamic sizes and zeta potentials are measured using dynamic light scattering on a Malvern Zetasizer Nano-ZS instrument. Zeta potential typically ranges from -100 mV to +100 mV, whereas values below -25 mV or above +25 mV usually have a high degree of stability, according to Shnoudeh et al. [86]. In this study, samples with zeta potentials in this range will hence be denoted as stable.

6.1 Citrate Coated Iron Oxide Nanoparticles

Citrate coated iron oxide nanoparticles (cIONPs) were synthesized according to the procedure described in section 5.1. The purpose of these particles was for use in the silanization process, which is discussed in section 6.2. Only citrate coated IONPs are used in this study. The reasoning for this decision is justified in section 6.2.2. In Figure 6.1 the color change when ammonium hydroxide was added to the reactor is shown, **(a)** shows the yellow/orange color of the iron salts dissolved in MQ water, and **(b)** shows the color of the reaction solution immediately after the ammonium hydroxide was added. The color change is due to the precipitation of magnetite, indicating that the nucleation happens immediately after the base is added.

(a) **(b)**

Figure 6.1: The color of the reaction medium during co-precipitation of IONPs **(a)** before ammonium hydroxide is added and **(b)** immediately after the base is added.

Initially, eight batches were synthesized, with the aim of mixing 3-4 of the batches with the most consistent properties. The purpose was to get a bigger batch to have the same base for easier comparison in the upcoming experiments where the particles would be used, i.e., in the silanization experiments performed later. The hydrodynamic sizes and zeta potentials for all the batches are shown in Figure 6.2, whereas the blue bars show the hydrodynamic sizes and the orange bars shows the zeta potential. As can be seen, the zeta potential for all batches is below -25 mV, indicating that these samples are stable in the aqueous solution. However, the hydrodynamic sizes show some variations. The deviations might be due to experimental error, for example, if the reaction mixture was exposed to air. The concentrations of the batches are shown in Table 6.1. Based on these measurements, B2, B3, B7, and B8 were mixed into one bigger batch, cIONPs-M1..

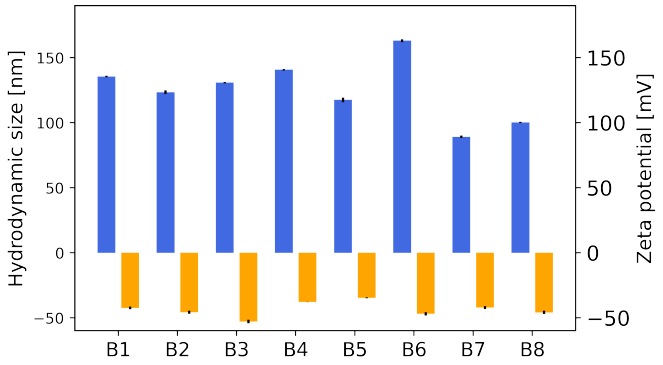

Figure 6.2: Hydrodynamic sizes and zeta potentials for B1-B8.

Table 6.1: Concentrations of the final products for B1-B9.

	B1	B2	B3	B4	B5	B6	B7	B8
C [mg/mL]	110±0	99±1	95±1	92±1	96±1	95±0	94±3	96±3

One of the main reasons to study IONPs is their unique properties, especially the superparamagnetic behavior. It is hence important to synthesize particles that easily separate when a magnetic field is applied. After mixing the batches, the particles were meant to be used for silanization experiments. However, when a small volume of the dispersion was added to an Eppendorf tube and placed on a permanent magnet, the particles did not separate. There were probably particles that did separate; however, it was impossible to distinguish these particles from the dark-colored supernatant. An image showing the Eppendorf next to the permanent magnet is shown in Figure 6.4 **(a)**. It is hypothesized that the sample contains by-products of other iron oxide species, for example, maghemite or hematite, which are less magnetic than the desired magnetite. Maghemite (γ-Fe_2O_3) is isostructural to magnetite but with higher oxidation state due to cation vacancies [62]. If magnetite is oxidized, maghemite or other non-stoichiometric, Fe^{2+}-deficient magnetite might arise. Maghemite is also ferrimagnetic, however, the magnetization saturation is decreased as a consequence of cation vacancies. Another explanation lies in the particle sizes; the activation energy for spin reversal scales with size, meaning a reduction of magnetization also occurs if the magnetite crystals exceed a certain size [62]. The suspicion of impurities of other iron oxide species could be further investigated by doing XRD measurements. However, since this study did not aim to study the formation of different iron oxide species during co-precipitation, it was decided not to include these measurements.

As a consequence, five new batches were prepared using the same co-precipitation method. The zeta potential and hydrodynamic sizes of these batches are shown in Figure 6.3. As shown in the figure, all samples are stable, as the zeta potentials are below 25 kV, and the hydrodynamic sizes are in the same range. The batches were carefully tested this time before mixing to check if the particles separated when exposed to a permanent magnet. The particles did separate for all the batches, however, for B11, the supernatant was a lot darker than for the other four batches. B9, B10, B12, and B13 were then mixed into a new big batch, cIONPs-M2. As can be seen from Figure 6.4 **(b)**, the particles in cIONPs-M2 did separate when placed next to the permanent magnet, and it was hence possible to remove the supernatant and subsequently use them in the silanization process. The hydrodynamic size and the zeta potential for cIONPs-M2 were 101±1 nm and -32±1 mV, respectively.

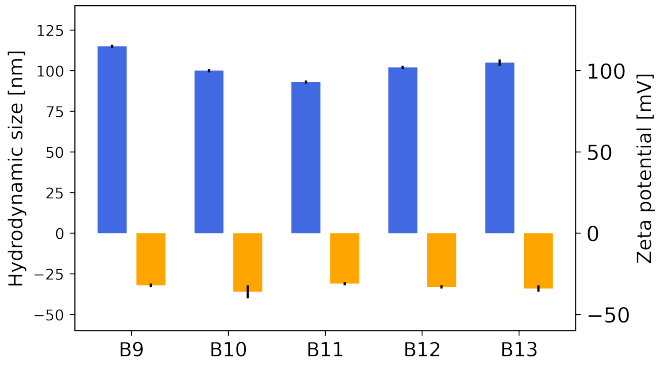

Figure 6.3: Hydrodynamic sizes and zeta potentials for B9-B13.

The magnetization properties for cIONPs-M2 were measured using VSM. The hysteresis loop is shown in Figure 6.5. The figure shows the moment as a result of the magnetic field. As can be seen from the figure, the hysteresis loop does not display magnetic remanence, and the sample reveals the recognizable hysteresis loop for superparamagnetic materials. The moment is zero when the magnetic field is removed, but the sample gets magnetized when exposed to a magnetic field. The particles are thus considered to be superparamagnetic. The magnetization saturation is 67 emu/g. This is in agreement with magnetization saturation values reported in the literature. In literature, the magnetization saturation of citrate coated IONPs is reported to be in the range from 55 emu/g to 75 emu/g [22, 25, 7].

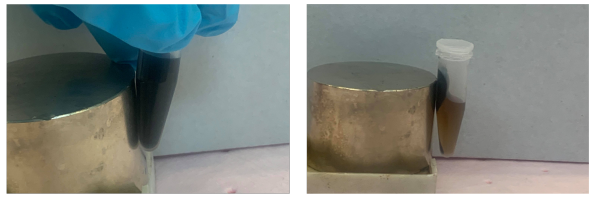

(a) **(b)**

Figure 6.4: Separation of cIONPs in the presence of a permanent magnet for two minutes for sample **(a)** cIONPs-M1 and **(b)** cIONPs-M2.

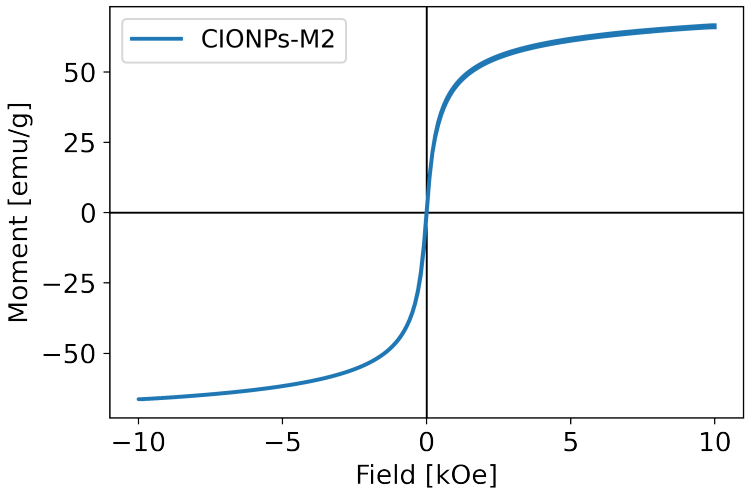

Figure 6.5: Magnetic properties of cIONPs-M2 measured by VSM.

6.2 Silica Coated Iron Oxide Nanoparticles

Silica coated cIONPs (ScIONPs) were synthesized according to the protocols described in section 5.2, using the cIONPs synthesized in section 6.1. This set of experiments are based on a previous study performed by Ali [4]. He studied the size and morphology of silica coated IONPs using a batch set up. In this study, the batch set up was replaced by a semi-batch set up.

6.2.1 Morphologies

Four different morphologies of ScIONPs were observed during this study. This is in agreement with the morphologies obtained by Ali [4]. In Figure 6.6 the different morphologies are defined with schematics and representative SEM observations. These definitions are reproduced and modified from the work of Ali [4] for easier comparison and discussion of the morphologies. The different morphologies are spheres/beads, incompletely fused particles, agglomerates, and irregularly shaped particles. In this chapter, the morphologies will be discussed using these terms.

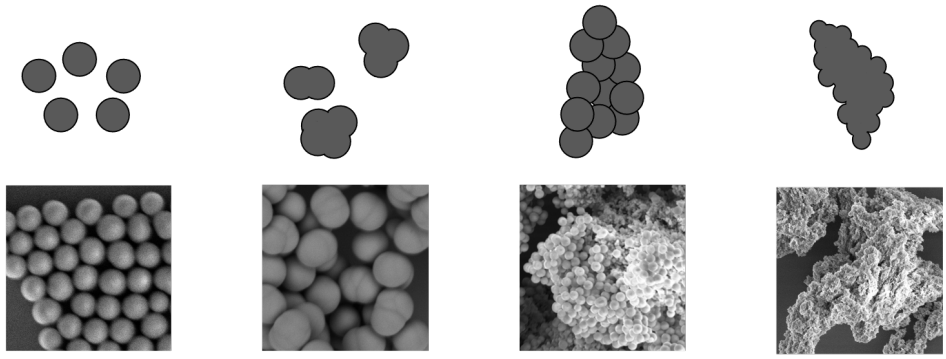

Figure 6.6: Different morphologies of ScIONPs observed during this study: (a) spheres/beads, (b) incompletely fused, (c) agglomerates and (d) irregular.

Energy dispersive spectroscopy (EDS) was used to investigate the chemical composition of the morphologies and to understand the successful coating of cIONPs. EDS measurements were on spherical particles and irregularly shaped particles. There are three possible products, ScIONPs, free silica, and magnetite. As the particles went through a total of 9 cleanings, with magnetic separation between each cleaning, it was expected that the particles did contain magnetic iron and that free silica had been disposed of. EDS was only performed on a single arbitrary sample, where both spherical particles and irregular particles were observed. It was assumed that the findings were consistent for all samples, although it might be different quantities of the elements in different samples.

An elemental mapping was performed on spherical particles and can be seen in Figure 6.7, where **(a)** shows the SEM image and **(b), (c)** and **(d)** suggest the distribution of iron, oxygen and silicon elements over the particles respectively. As suggested by the analysis, all the expected elements are present in the particles. From the images, it seems like all of the three elements are present throughout the particles, which means that core-shell structures are not obtained but rather iron distributed throughout the silica matrix.

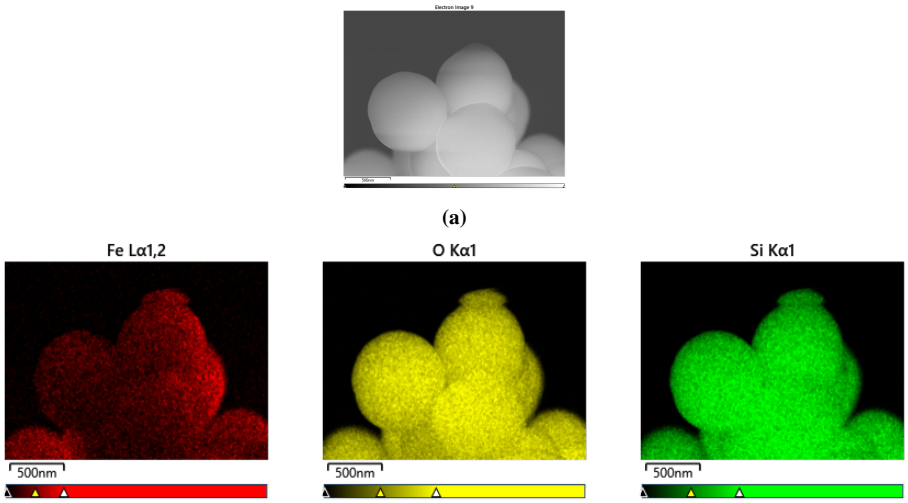

Figure 6.7: Elemental mapping of spherical particles using EDS.

A line profile through a single spherical particle is shown in Figure 6.8. It shows the count per second through the length of the particle, marked with a yellow line. In agreement with the mapping analysis, the line profile suggests that iron, oxygen, and silicon are present in the particles. The ratio of silicon and oxygen content to iron content seems to be very high. This is expected when considering the ratio of iron to silicon added to the reaction mixture, which is 0.07 on a molar basis. However, it needs to be emphasized that EDS is not performed quantitatively, and the distribution only gives an idea of the content.

A line profile was also performed through an irregular particle and is shown in Figure 6.9. The analysis shows that iron, oxygen, and silicon are all present with the same low iron to silicon content as for the line profile of a single sphere.

Hence, it is shown that the particles obtained in this study are the desired silica coated iron oxide nanoparticles.

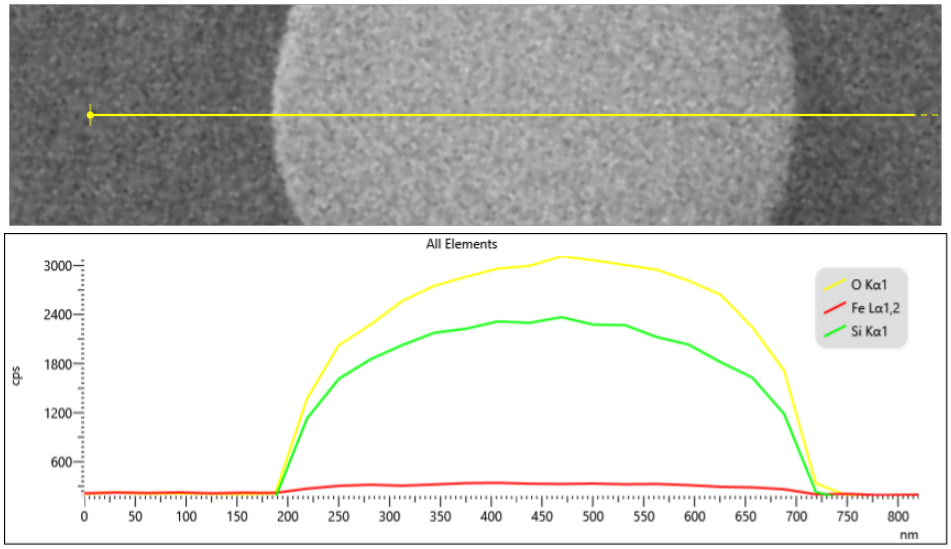

Figure 6.8: A line profile, showing the chemical composition, through a single spherical particle, measured by EDS.

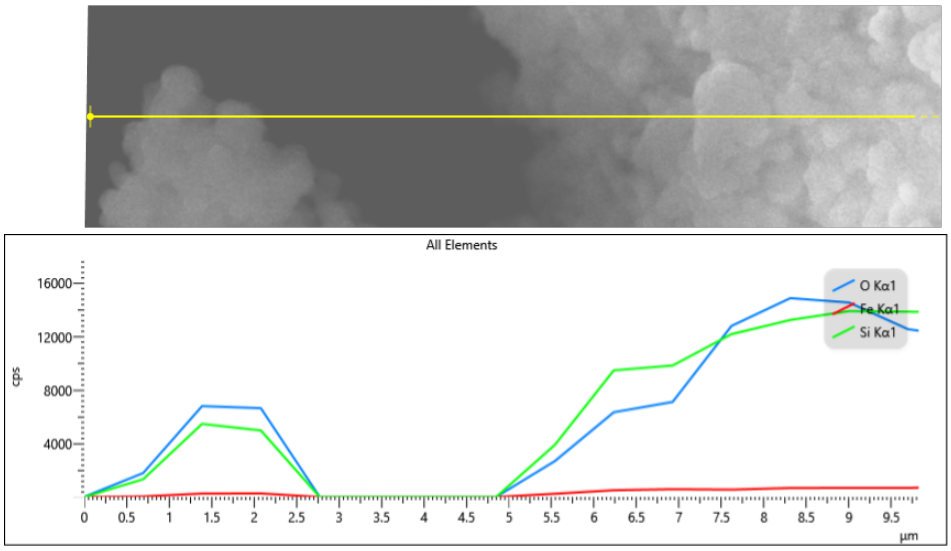

Figure 6.9: A line profile, showing the chemical composition, through an irregular particle, measured by EDS.

In the following sections, different parameters affecting the particle size and morphology are discussed. All particle sizes are obtained by analysis of SEM images using ImageJ.

The sizes are measured by counting ∼200 random particles in different areas of the images. The sizes are only measured for samples where spheres, incompletely fused or agglomerates are observed, as the irregular particles do not reveal a defined structure. It must be stressed that there are challenges with size determination using SEM images, such as imaging the particles in the dried state, ignoring agglomerates, and counting particles manually. All particle sizes are rounded off to the nearest 1 nm due to uncertainty in the measuring technique. The polydispersity index (PDI) is calculated using the formula reported by Pusey [78], i.e., dividing the standard deviation by the mean particle size. However, before starting the experiments, the reaction conditions needed to be selected.

6.2.2 Reaction Conditions

The proposed approach for the silanization of cIONPs in this study was to make an experimental design using JMP. Firstly, the reaction parameters needed to be selected. In the work performed by Ali [4], nature of the solvent, use of citrate coated versus non-coated IONPs, the concentration of ammonium hydroxide, and mass of IONPs/cIONPs were used as reaction parameters. For the experiments in this study, it was decided to combine the parameters Ali used and new parameters following the semi-batch procedure. This was decided to compare the effect of using a semi-batch set up rather than a batch process.

The first decision to make was for how long period the reactions should proceed. For all silanization experiments, it was decided to leave the reaction for 5 hours. That is the same reaction time used by Ali [4]. In literature, a wide range of reaction times are reported. However, Ali found that after 5 hours, 90% of the mass was converted, and the morphologies obtained were similar to what was obtained after 24 hours. This means that a high yield is achieved after only 5 hours, and to convert the remaining 10%, a long period was required. Using only 5 hours of reaction was thus chosen.

Secondly, the decision if either coated or non-coated IONPs should be used had to be made. The choice was based on the results obtained by Ali. He reported that the number of agglomerates increased by a significant degree when non-coated IONPs were used, as compared to cIONPs. The PSD for non-coated IONPs was also broader than for cIONPs [4]. It was hence decided only to use cIONPs in this study. It was also decided to proceed with the same masses as Ali's, 25 mg, 50 mg, and 75 mg.

The use of which solvents to use in this study had to be decided as well. Ali used isopropanol and ethanol in his study and got particles of different sizes and morphologies. Experiments with isopropanol gave bigger particles than with ethanol. However, there were some deviations due to the formation of incompletely fused particles [4]. It was thus decided to proceed using both solvents for the semi-batch set up.

The new parameters in the semi-batch process were the flow rates of ammonium hydroxide and TEOS. It was decided to use the same amount of TEOS as Ali, 2 mL. There is literature on the semi-batch set up of modified Stöber methods introducing TEOS over time. However, to elect flow rates of ammonium hydroxide, it was concluded that some initial experiments were necessary, which is described in section 6.2.3.

6.2.3 Effect of Ammonium Hydroxide Flow Rate

As there is limited literature discussing studies where ammonium hydroxide is added over some time in the Stöber method, three semi-batch experiments were performed initially to investigate how the flow rate would affect the final particle size and morphology.

It was decided to use a total amount of 3.5 mL of ammonium hydroxide for the initial experiments. This choice was yet again based on the parameters used by Ali [4]. It is the middle value of Ali's concentrations in the batch experiments, which were 0.5 mL, 3.5 mL, and 6 mL ammonium hydroxide. It was also decided to do the initial experiments in isopropanol, using the middle value of cIONPs mass, 50 mg. As these experiments were performed to study the effect of the flow rate of ammonium hydroxide, TEOS was added at once, similar to a batch experiment set up.

The ammonia hydroxide was added using a syringe pump. It was decided to add the ammonium hydroxide over a specific time rather than choosing a specific flow rate to better control the rate. Three different time intervals were chosen, 60 min, 30 min, and 15 min corresponding to flow rates of 0.06 mL/min, 0.12 mL/min, and 0.23 mL/min, respectively. The start of the reaction was defined as when the first drop of ammonium hydroxide was added to the reactor, giving the same total time of 5 hours for all reactions. The reaction parameters are summarized in Table 6.2.

Table 6.2: Reaction parameters in the initial semi-batch experiments.

Solvent	Mass of cIONPs [mg]	TEOS [mL]	NH_4OH [mL/min]	Time of addition min
Isopropanol	50	2	0.06	60
Isopropanol	50	2	0.12	30
Isopropanol	50	2	0.23	15

The concentration profiles of the ammonium hydroxide over time, for the three experiments, are shown in Figure 6.10. Higher molarity of ammonium hydroxide is achieved faster for the faster flow rate, and a higher pH value is expected earlier during the reaction, however, it is not known if and so how fast the hydroxide ions are consumed, so pH measurements during the addition is required to say this for sure. However, at the end of the reaction, the same total amount of ammonium hydroxide is added; if no hydroxide were consumed, the final pH would be expected to be identical for the three cases. The fact that hydroxide ions might decrease as the reaction proceeds is not appraised in these graphs. It would be interesting to look at how pH varies over time to see how fast the excess hydroxide ions are consumed and investigate the reaction's kinetics. In this way, it might be possible to control the pH over time, which can help tune the particle properties.

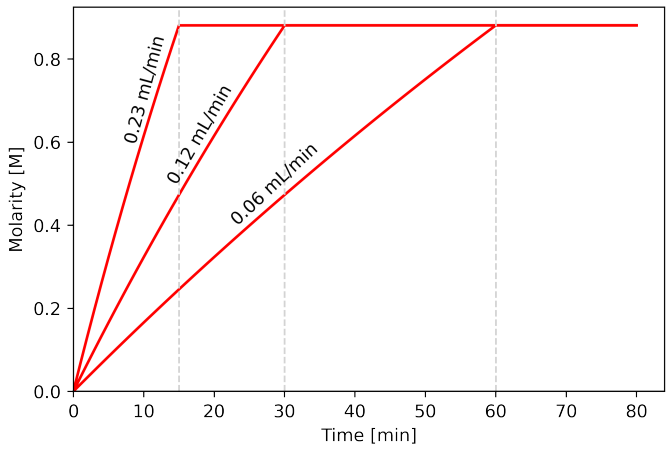

Figure 6.10: Concentration profile for NH_4OH for experiments performed using three different flow rates, 0.06 mL/min, 0.12 mL/min and 0.23 mL/min.

Figure 6.11, 6.12 and 6.13 shows the SEM images of the experiments performed with flow rates of 0.06 mL/min, 0.12 mL/min and 0.23 mL/min respectively. By studying the SEM images, it can be seen that there are no big deviations in the morphology obtained in these three experiments as spheres, agglomerates, and irregularly shaped particles are observed for all. The sizes calculated from the SEM images are 737±38 nm, 813±78 nm, and 982±73 nm for flow rates of 0.06 mL/min, 0.12 mL/min and 0.23 mL/min respectively, with corresponding PDIs of 0.05, 0.1 and 0.07. The sizes, as a result of the ammonium hydroxide flow rates and the PSDs, are shown in Figure 6.14. The bar showing flow rate equal to zero is the mean size obtained in the batch experiments performed by Ali [4], keeping the other parameters constant, the size was reported to be 983±47 nm. As can be seen from **(a)**, smaller sizes are obtained using a lower flow rate of ammonium hydroxide. The same mean size is obtained for the highest flow rate of ammonium hydroxide and the batch process. By studying the PSDs in **(b), (c)** and **(d)**, it can be seen that a narrower size distribution is observed for the slowest addition of ammonium hydroxide.

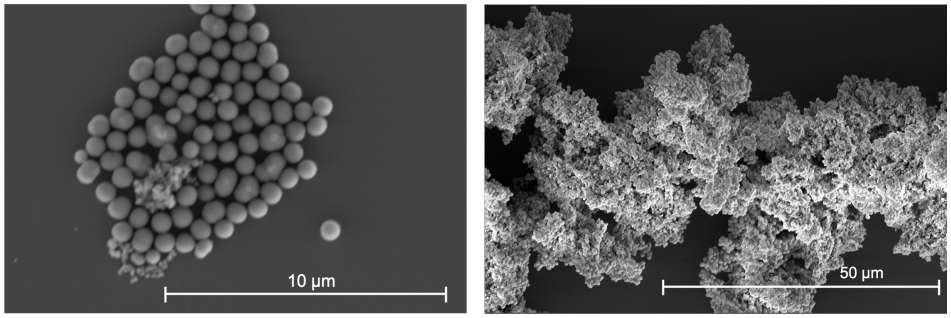

(a) **(b)**

Figure 6.11: SEM images for experiment where a flow rate of 0.06 mL/min of ammonium hydroxide is used.

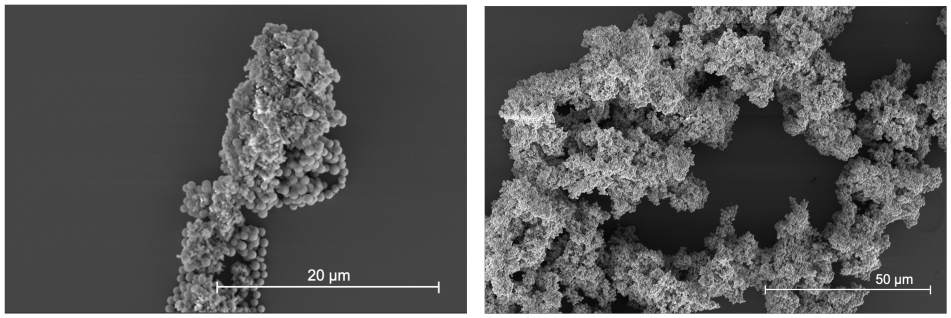

(a) **(b)**

Figure 6.12: SEM images for experiment where a flow rate of 0.12 mL/min of ammonium hydroxide is used.

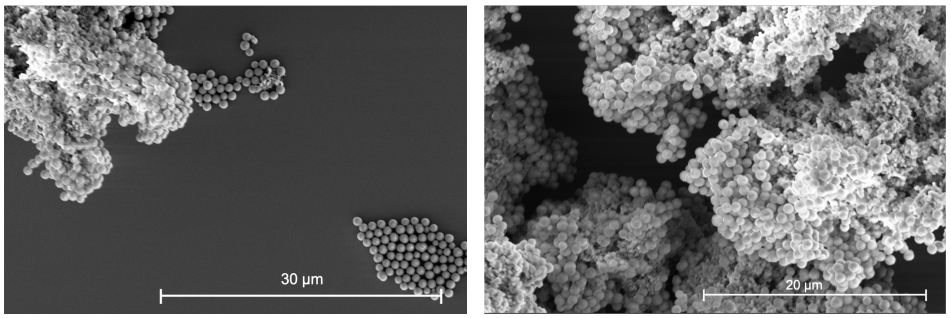

(a) **(b)**

Figure 6.13: SEM images for experiment where a flow rate of 0.23 mL/min of ammonium hydroxide is used.

The final particle sizes are a result of the hydrolysis and condensation rate in the Stöber process as described in section 4.2. Han et al. [34] report that a low concentration of ammonium hydroxide results in small particles with a broad size distribution as a consequence of lowered TEOS hydrolysis rate. At higher concentrations, the particles are bigger but with a narrower size distribution as the nucleation step is rapid. When ammonium hydroxide is added in one portion, the concentration of hydroxide ions will decrease as it is consumed. In these experiments, the total amount of ammonium hydroxide is added at a constant rate over some time, giving possibilities to control the pH of the solution using different flow rates. Dabbaghian et al. [1] state that an increase of ammonium hydroxide increases the size of the particles until a certain level where the sizes start decreasing because the condensation rate increases, which may be the reason for the bigger sizes obtained at higher flow rates.

As explained in section 2.2.3, the growth of particles consists of two processes, reaction-controlled or diffusion-controlled mechanisms. The kinetics of the growth process is essential for the final particle size distribution. If the growth process is appropriately controlled, the formation of uniformly sized particles can be achieved [31]. The difference in radius decreases with a prolonged growth time when the growth is controlled by diffusion. In this set of experiments, the smaller size and narrower size distribution obtained with a lower flow rate of ammonium hydroxide can be explained by a diffusion-controlled process. When the ammonium hydroxide in these experiments is supplied at a lower flow rate, the reaction is slow, and the supply of growth species becomes slow as well. By attaining a low concentration of growth species, it is possible to maintain a diffusion-controlled growth mechanism. The diffusion distance, in this case, would be more significant, and diffusion would become the limiting step.

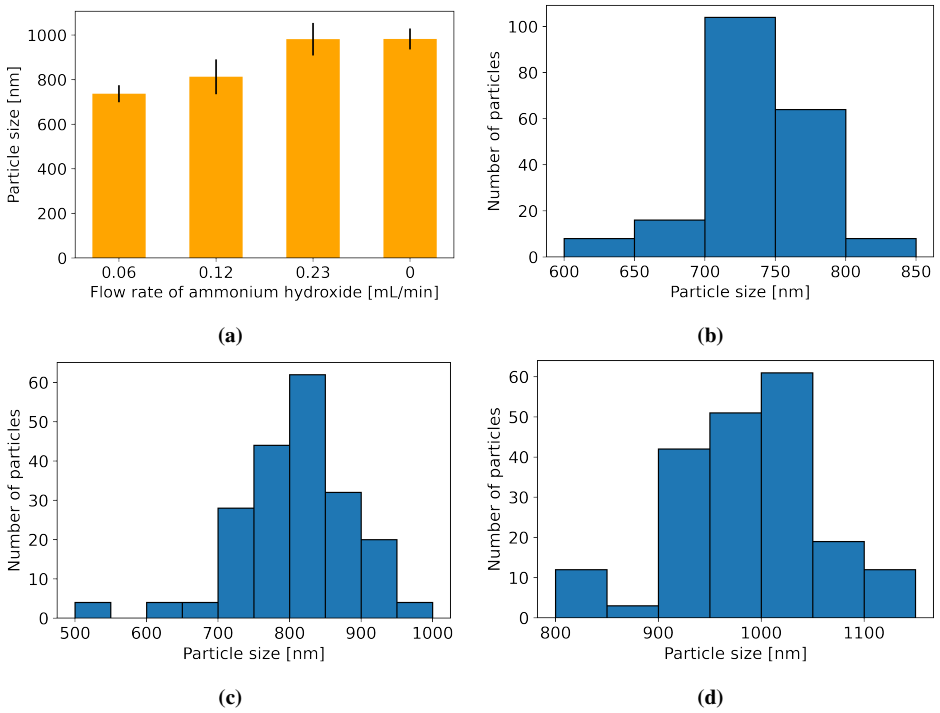

Figure 6.14: Measurements of the particle sizes obtained in the initially experiments, where **(a)** is the mean particle sizes, as a result of the ammonium hydroxide flow rate, mean size from the batch experiment corresponds to the column where ammonium hydroxide flow rate is zero and is obtained from the study performed by Ali [4]. **(b), (c)** and **(d)** show the PSDs for ammonium hydroxide flow rates of 0.06 mL/min, 0.12 mL/min and 0.23 mL/min respectively.

Based on these results, it was hypothesized that the flow rate of ammonia has a significant effect on particle size. However, more investigations need to be performed to draw any conclusions. However, it was decided to proceed with semi-batch experiments adding ammonium hydroxide for 60 minutes due to the smaller sizes obtained and the higher degree of monodispersity.

6.2.4 Experimental Design

As explained in the methodology chapter, a custom design was made using JMP. The reaction parameters used in this design are based on a previous batch study performed by Ali [4], as explained in section 6.2. The reaction was carried out for 5 hours using the same solvents as Ali, isopropanol, and ethanol. Similar masses of cIONPs are used, 25 mg, 50 mg, and 75 mg. The flow rates of ammonium hydroxide that are used are 0.1 mL/min, 0.054 mL/min, and 0.008 mL/min, whereas the highest and lowest flow rates correspond to the highest and lowest volume of ammonium hydroxide used in Ali's batch study, 6

mL and 0.5 mL when adding for 60 minutes. The middle value, 0.054 mL/min, is the highest and lowest flow rate average. This flow rate gave a total volume of ammonium hydroxide of 3.2 mL. The amount of TEOS was kept constant, 2 mL; however, the flow rates were decided to be 0.03 mL/min and 0.08 mL/min. The lowest flow rate was chosen because TEOS would then be added for the exact total time, i.e., 60 minutes, as ammonium hydroxide. The highest flow rate was chosen to be the middle value of the two highest flow rates of ammonium hydroxide, 0.054 mL/min and 0.1 mL/min.

In JMP, a custom design was chosen, meaning that all combinations of parameters are not included as they would be in a full factorial design. A custom design constructs optimal design custom-built for an experimental setting that is more cost- and time-efficient than a full factorial design. The design of experiments is presented in section 5.2.3. Although the design of experiments gave a good understanding of the influence of different reaction parameters, a couple of more experiments were included to get a bigger overview. This will be explained in the following sections.

For easier discussion, the sample names are based on the reaction parameters fixed in the specific experiments, as described in section 5.2.3. It is repeated here; the sample names consist of a letter followed by two numbers, and lastly, another letter. The first letter is either 'I' for isopropanol or 'E' for ethanol. The first number represents the mass of cIONPs in milligrams, 25, 50, or 75. The second number represents the ammonium hydroxide flow rate and is either 0.1, 0.054, or 0.008. The last letter represents the flow rate of TEOS and is either 'L' for low flow rate, 0.03 mL/min, or 'H' for high flow rate, 0.08 mL/min. For example, for sample I-25*0.1-L, the reaction parameters would be isopropanol as solvent using 25 mg cIONPs, an ammonium hydroxide flow rate of 0.1 mL/min, and a TEOS flow rate of 0.3 mL/min. A table with all experiments is attached in Chapter 5.

6.2.4.1 Molarity Profiles

The built-up of the semi-batch setup concentrations is essential to understand the nucleation and growth processes. In Figure 6.15 **(a)-(f)** the concentration profiles for the different combinations of flow rates of ammonium hydroxide and TEOS are shown up to 60 minutes of the reaction, after which the concentrations will remain constant. The fact that ammonium hydroxide and TEOS are consumed during the reaction is not taken into consideration. The consumption of the reactants could be studied by doing pH measurements during the reaction.

As can be seen from the graph, for the cases where TEOS is added at the rate of 0.03 mL/min, both TEOS concentration and ammonium hydroxide concentration are increasing until 60 minutes is reached. When TEOS is added at the rate of 0.08 mL/min, the concentration of ammonium hydroxide increases up to 60 minutes, and the concentration of TEOS increases up to 25 minutes, after which it starts decreasing slightly due to more addition of ammonium hydroxide. It should also be noticed that for all cases, except when the lowest flow rate of ammonium hydroxide, the concentration is higher for ammonium

hydroxide than for TEOS.

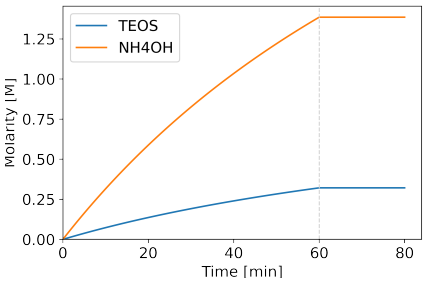

(a) 0.1 mL/min NH_4OH and 0.03 mL/min TEOS

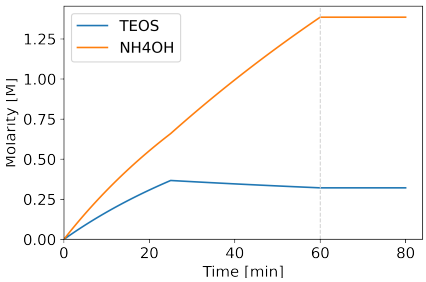

(b) 0.1 mL/min NH_4OH and 0.08 mL/min TEOS

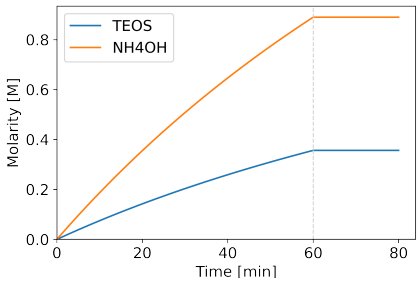

(c) 0.054 mL/min NH_4OH and 0.03 mL/min TEOS

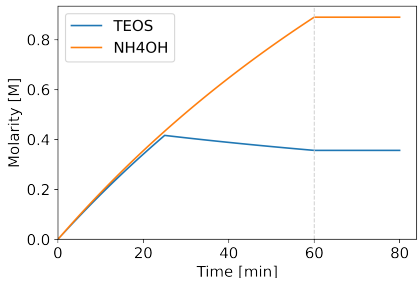

(d) 0.054 mL/min NH_4OH and 0.08 mL/min TEOS

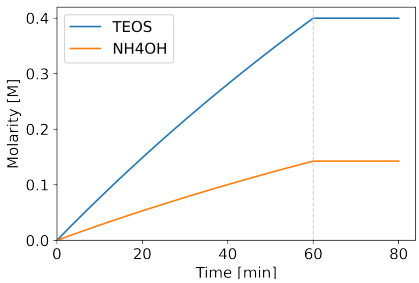

(e) 0.008 mL/min NH_4OH and 0.03 mL/min TEOS

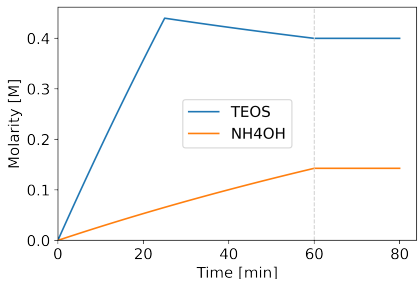

(f) 0.008 mL/min NH_4OH and 0.08 mL/min TEOS

Figure 6.15: Concentration profiles for experiments using different combinations of ammonium hydroxide and TEOS flow rates.

6.2.4.2 Effect of Ammonium Hydroxide Concentrations and Flow Rates

In this study, three different concentrations of ammonium hydroxide are used. For all semi-batch experiments included in the experimental design, the ammonium hydroxide was added over a time interval of 60 minutes. The volumes used were 0.5 mL, 3.2 mL and 6 mL, which correspond to flow rates of 0.008 mL/min, 0.054 mL/min and 0.1 mL/min,

respectively.

In the experiments performed by Ali [4], only irregular particles were observed when the lowest volume of ammonium hydroxide, 0.5 mL, was used. Although no spherical particles were observed in the batch experiments using 0.5 mL ammonium hydroxide, it was decided to use the same volume in the semi-batch process to see if adding it over time would affect the final morphology.

A total of six experiments were conducted using the lowest flow rate of ammonium hydroxide, 0.008 mL/min, i.e., using a total volume of 0.5 mL ammonium hydroxide. In these experiments, the molarity of ammonium hydroxide in the final solution was 0.14 M. The concentration profiles for these experiments are shown in Figure 6.10(e) and (f). As can be seen from these graphs, the molarity of ammonium hydroxide is lower than the molarity of TEOS during the whole reaction.

SEM images of I-75*0.008-L and E-25*0.008-L are shown in Figure 6.16, where 0.03 mL/min TEOS is used and 75 mg and 25 mg of IONPs respectively. By studying the SEM images, no spherical particles or agglomerates are observed, only irregular shaped particles. It is thus not possible to measure the particle sizes. These findings were coherent for all experiments using the low flow rate of ammonium hydroxide.

It was proposed by Qie et al. [79] that a low concentration of ammonium hydroxide leads to irregular particles due to incompletely hydrolyzed TEOS. It must be emphasized that Qie et al.'s studies are based on batch processes, however, this is also applicable for the semi-batch process. TEOS is a tetrahedral molecule consisting of a silicon atom surrounded by four ethoxy groups. Qie et al. state that when ammonium hydroxide is in excess, fully hydrolyzed species are produced, $Si(OH)_4$, making the particle grow evenly. On the other hand, when the concentration of ammonium hydroxide is low, incompletely hydrolyzed species are formed, making the particle grow unsymmetrical.

Another reason for the formation of irregular particles at low ammonium hydroxide concentrations was proposed by Herbert Giesche [29]. At low ammonium hydroxide concentrations, the particles are not adequately stabilized due to the too low surface potential of the particles. The low stability of the dispersion leads to the agglomeration of the particles.

Hence, both the batch and the semi-batch process gave irregular shaped particles at the lowest volume of ammonium hydroxide. No further experiments using the lowest volume of ammonium hydroxide were thus performed.

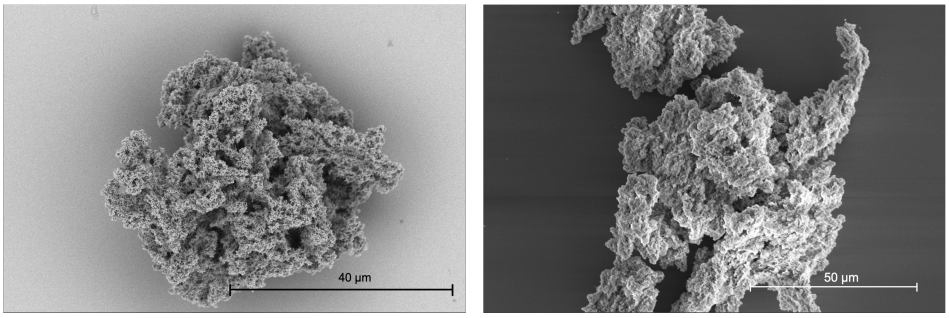

(a) **(b)**

Figure 6.16: SEM images for experiment (a) I-75*0.008-L and (b) E-25*0.008-H.

For the experiments where the two higher flow rates, 0.054 mL/min and 0.1 mL/min, with corresponding volumes of ammonium hydroxide 3.2 mL and 6 mL, spherical particles together with irregularly shaped particles were observed. The particle sizes were hence possible to measure. As can be seen from the molarity profiles in Figure 6.15, what differentiates these experiments from the low ammonium hydroxide flow rate experiments, is that the molarity of ammonium hydroxide is higher than the molarity of TEOS during the whole reaction. Figure 6.16 shows the SEM images of experiment, **(a)** I-75*0.1-L and **(b)** I-50*0.054-L. The sizes obtained by the SEM images were 10170$\pm$120 nm and 873$\pm$97 nm, respectively. It should be mentioned that different masses of cIONPs, 75 mg and 50 mg, are used for those two experiments; however, as will be discussed later, the mass in these experiments did not have a significant effect on the particle sizes. The particle sizes obtained at 0.1 mL/min and 6 mL of ammonium hydroxide are bigger than the sizes obtained at 0.054 mL/min and 3.2 mL of ammonium hydroxide. This is not in agreement with the batch studies performed by Ali [4], where it is reported that for most cases, the particle size decreases with the increase in the concentration of ammonium hydroxide. It should be mentioned that more experiments should be performed before stating the trend in the semi-batch experiments. However, these result, i.e., increase in size with an increase in ammonium hydroxide is consistent with several studies reported in the literature. Han et al. [34], Ibrahim et al. [84] and Qie et al. [79] found that the particle sizes increased with the increase in ammonium hydroxide concentration. Ibrahim et al. state that an increase of ammonium hydroxide increases the hydrolysis and condensation rate. A high hydrolysis rate will lead to a rapid increase in the concentration of the intermediate, $Si(OEt)_{4-x}(OH)_x$. When the barrier for nucleation is reached, the consumption of the intermediate is fast, which gives rapid nucleation. This gives less number of nuclei, and bigger particles [84].

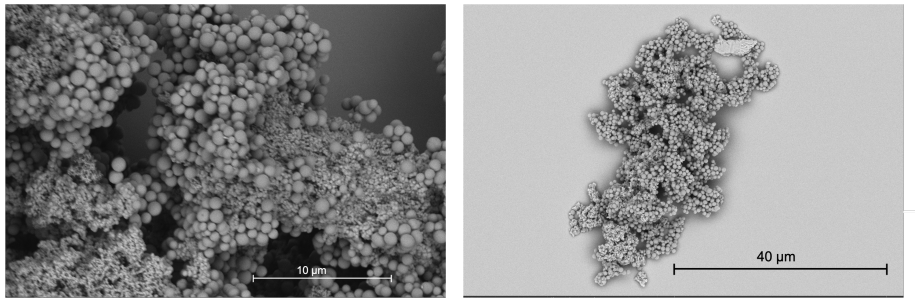

(a) **(b)**

Figure 6.17: SEM images for experiment (a) I-75*0.1-L and (b) I-50*0.054-L.

As the PDIs for these experiments were relatively high, 0.12 and 0.11, for I-75*0.1-L and I-50*0.054-L, respectively, it was decided to investigate the possibility to reduce the polydispersity of the sample where 6 mL of ammonium hydroxide was used, like in the initial experiments in section 6.2.3. An extra experiment was hence introduced using new reaction parameters.

New experiment

An extra experiment was introduced to see if the PDI of I-75*0.1-L could be reduced. It was decided to use the same amount of ammonium hydroxide, 6 mL, however, using an even slower flow rate. The middle flow rate, 0.054 mL/min, was used. This means that the total volume of ammonium hydroxide, 6 mL, would be added for 111 minutes instead of 60 minutes. This sample is called I-75*0.054(6)-L, where (6) indicates that the total volume is 6 mL and not 3.2 mL, as it would be for the original experiments. The result is consistent with the result obtained in the initial experiments on the flow rate of ammonium hydroxide. The mean size was smaller for the lower flow rate, 840$\pm$80 nm, as compared to the higher flow rate where the size was 1020$\pm$120 nm. The PSDs for I-75*0.1-L and I-75*0.054(6)-L are shown in Figure 6.18. As can be seen from the figure, the PSD is more narrow for the experiment using a lower flow rate of ammonium hydroxide. The same reason applies here as in the initial experiments. The ammonium hydroxide, which is the catalyst, is used to control the growth rate and the supply of growth units, leading to smaller particle sizes and increasing the degree of monodispersity. By attaining a slower flow rate of ammonium hydroxide, the concentration of growth species is lower, leading to slower growth. In this way, it is possible to maintain a diffusion-controlled growth mechanism, where the diffusion distance is more significant, and diffusion is the limiting step.

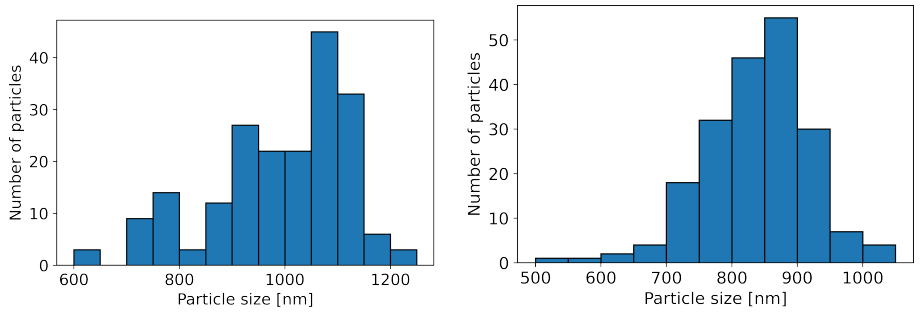

(a) **(b)**

Figure 6.18: PSD for **(a)** I-75*0.1-L and **(b)** I-75*0.054(6)-L

6.2.5 Effect of Solvent

The experiments in this study were performed using two different solvents, isopropanol, and ethanol. Experiments performed using the same reaction conditions, just varying the solvent gives different morphology. It is observed that spherical particles are more frequently observed when isopropanol is used as the solvent. On the other side, the experiment with the smallest obtained mean particle size is carried out in ethanol.

In some experiments where the same conditions are used, just varying the solvent, isopropanol gives beads and agglomerates while ethanol only reveals irregular shaped particles. I-75*0.1-L and E-75*0.1-L are examples where these findings are observed. SEM images of these experiments are shown in Figure 6.19. By studying the SEM images, a couple of spherical particles are spotted for the experiment using ethanol. However, the number is significantly lower than the number of spherical particles observed in the corresponding experiment using isopropanol. The number is also too low to count the particles and measure the size. These findings are not consistent with the batch process where beads are usually observed in both solvents.

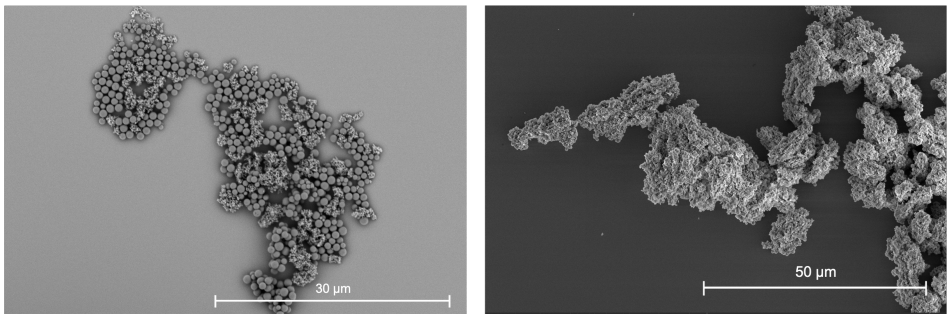

(a) **(b)**

Figure 6.19: SEM images for **(a)** I-75*0.1-L and **(b)** E-75*0.1-L

In the batch experiments performed by Ali [4], bigger particle sizes are obtained using isopropanol, except for some experiments, which resulted in incompletely fused and hence bigger particles. Comparing two experiments from this study, E-50*0.054-H and I-50*0.054-H, where 0.054 mL/min ammonium hydroxide, 0.08 mL/min TEOS, and 50 mg of IONPs are used, we can see from Figure 6.20 that the size of E-50*0.054-H, 750±40 nm, is smaller than the size of I-50*0.054-H, 960±70 nm. This is hence in agreement with the batch experiments. The PDIs are 0.05 and 0.07 respectively and the particle size distributions are shown in Figure 6.20 **(b)** for the ethanol experiment and **(c)** for the isopropanol case. For both experiments, spheres and irregularly shaped particles are observed. The particle size distribution is more narrow for the ethanol case, which is coherent with the particle size distributions from the batch experiments by Ali [4].

For another set of experiments where all parameters are kept constant except the type of solvent, whether ethanol or isopropanol is used does not affect the resulting particle sizes. This is observed for experiment E-50*0.054-L and I-50*0.054-L, where the SEM sizes are 870±90 nm and 870±100 nm for the samples, respectively, and both having a PDI of 0.11. The sizes are shown in Figure 6.20. Spheres and aggregates are observed in both cases.

The differences in morphology and particle sizes using different solvents might be due to the structure of the alcohols. It is proposed in the literature that the kinetics of the reactions are a result of the polarity and steric hindrance of the alcohol. If the polarity is the determining factor, ethanol, which is more polar than isopropanol, will slow down the reaction due to the formation of hydrogen bonds with the hydroxide ions. This might explain the irregular particles obtained in the experiments where spherical particles are not obtained in ethanol. If ethanol forms hydrogen bonds with the hydroxide ions, less hydroxide is available for TEOS hydrolysis. This can be related to the low concentration of ammonium hydroxide in section 6.2.4.2. Incompletely hydrolyzed TEOS might result in unsymmetrical particle growth.

However, if the steric hindrance is the determining factor, ethanol will speed up the reaction due to the shorter carbon chain. A lot of reported studies [13] states that it is not easy to draw any conclusions on the kinetics of the reactions based on different solvents used. The results can, in many cases, not be explained by only looking at single properties. However, the combination of many factors, such as viscosity and solvation, in addition to the factors already mentioned. Based on the results from this study and results obtained from literature, it seems like the use of solvent in many cases needs to be investigated using a trial-and-failure approach.

Because many experiments in ethanol did not allow finding the sizes, the final model fitting on particle sizes, which is presented in section 6.2.6, does not contain many experiments with ethanol. However, as mentioned before, the experiment with the smallest obtained particles is synthesized in ethanol, meaning that ethanol should not be excluded from future experiments.

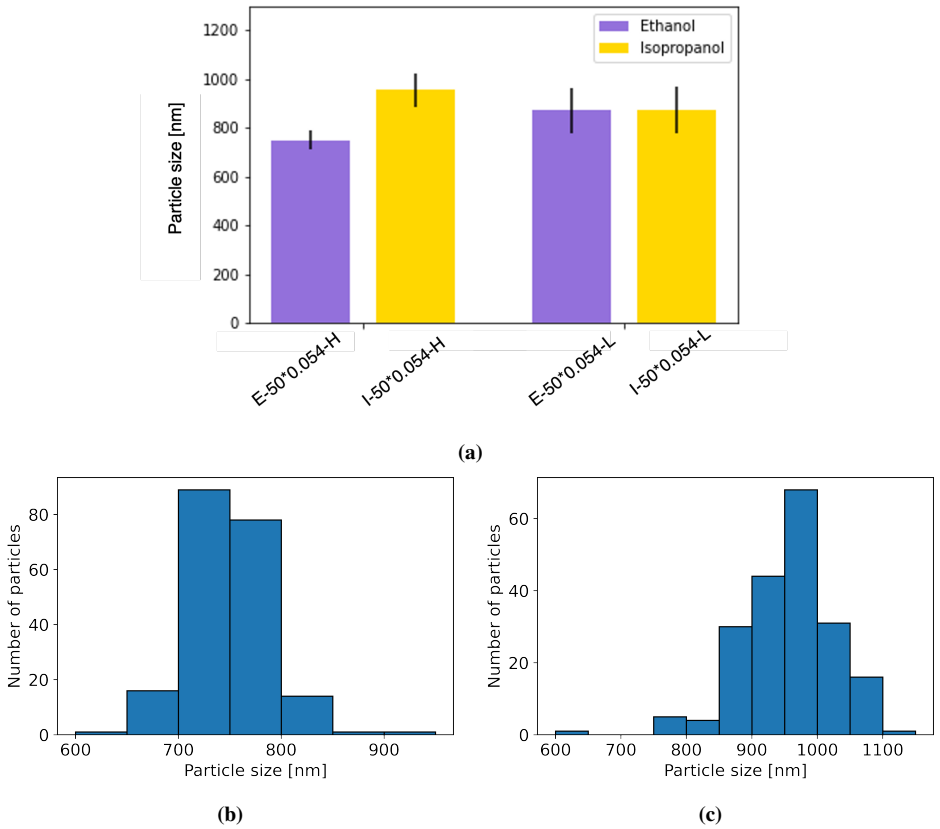

Figure 6.20: **(a)** Particle sizes obtained using different solvents, and PSDs for **(b)** E-50*0.0054-H and **(c)** I-50*0.0054-H

6.2.5.1 Effect of cIONPs Mass

The different masses of cIONPs used in this study were 25 mg, 50 mg, and 75 mg. By analysis of SEM images of the final particles, it can be seen that the mass of cIONPs is a vital parameter mainly for the morphology of the particles.

In experiments I-25*0.1-L and I-75*0.1-L, where type of solvent, ammonium hydroxide flow rate, and TEOS flow rate are kept constant, 25 mg and 75 mg IONPs were used, respectively. The sizes obtained with 25 mg, 1058$\pm$81 nm, are bigger than the sizes where 75 mg was used, 1017$\pm$120 nm. The reason for the difference in size is the morphologies obtained. With the use of 25 mg cIONPs, incompletely fused particles like doublets, triplets and quartets are observed together with spherical particles; however, when 75 mg of cIONPs were used, only spheres were observed. In both cases, aggregates were also

present. SEM images for the two experiments are shown in Figure 6.21 for the use of 25 mg cIONPs and Figure 6.22 when 75 mg cIONPs was used.

I-25*0.1-L was repeated to see if incompletely fused particles were still the outcome to confirm the repeatability of the conditions. The particles still revealed the same morphology. The same observations were also found in I-25*0.1-H and I-75*0.1-H, incompletely fused particles for the experiment where 25 mg cIONPs were used, and spheres when 75 mg cIONPs were used; this again confirms the trend.

From these results, it seems like, with 25 mg of cIONPs, the ratio of IONPs to TEOS is low. Zerrouki et al. [100] claimed that a relative fraction of 2-4 particle aggregates might be controlled by the concentration of silica in the medium. In these experiments, the ratio of cIONPs to TEOS varies with a factor of 2 and 3, from 25 mg to 50 mg and 75 mg, as the final volume of TEOS is constant. Another explanation is the less surface area of seeds available in the suspension. The silanol monomers have thus smaller areas to grow on, which might interrupt the growth of perfect spheres. Herbert Giesche [29] used seed dispersion of silica for the growth of silica particles and proposed that highly diluted seed dispersions increased the diffusion distance of hydrolyzed TEOS to the particle surface, increasing the probability of agglomeration and formation of doublet particles.

If the aggregation barrier between the particles is not significant, the probability of the occurrence of two particles aggregating in each collision is increasing [74]. That might be due to electrostatic or steric stabilization. The collisions arise due to the Brownian movement in the reaction medium and the van der Waals attraction. The probability of such aggregations decreases with increasing repulsive potential. Hence, it is hypothesized that a higher concentration achieved by using 50 mg or 75 mg of IONPs increases the repulsive potential in the solution.

A new experiment using the same parameters as in I-25*0.1-L and I-75*0.1-L, only with 50 mg cIONPs, I-50*0.1-L, was performed to see if this would result in incompletely fused and spherical particles. The resulting morphology was spherical particles, indicating that the incompletely fused particles occur somewhere between 25 mg and 50 mg cIONPs. The particle sizes are shown in Figure 6.23. The figure shows that the difference in mean particle size obtained for 50 mg and 75 mg of cIONPs is negligible. In the batch experiments, larger particle sizes are obtained for higher amounts of cIONPs, meaning that the particle sizes produced during a semi-batch process are easier to control when higher amounts of cIONPs are used.

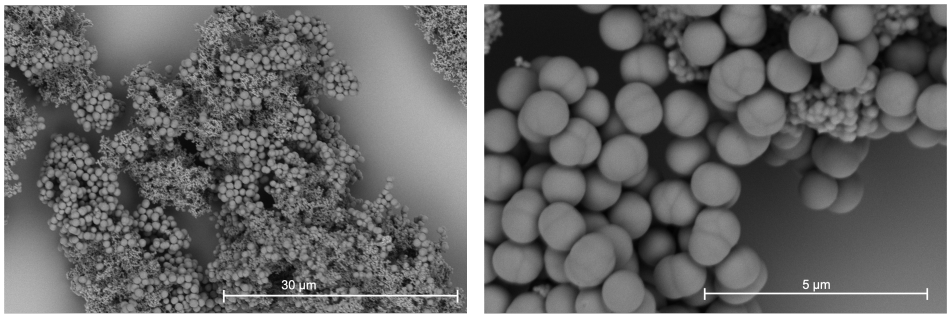

Figure 6.21: SEM images for experiment I-25*0.1-L showing incompletely fused particles and irregular particles.

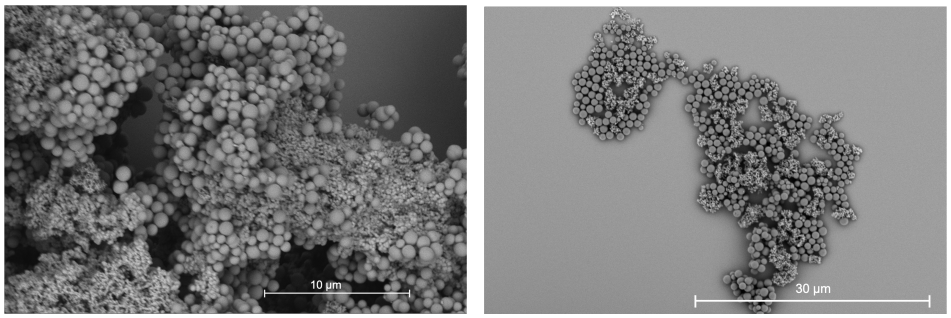

Figure 6.22: SEM images for experiment I-75*0.1-L showing spherical particles and irregular particles.

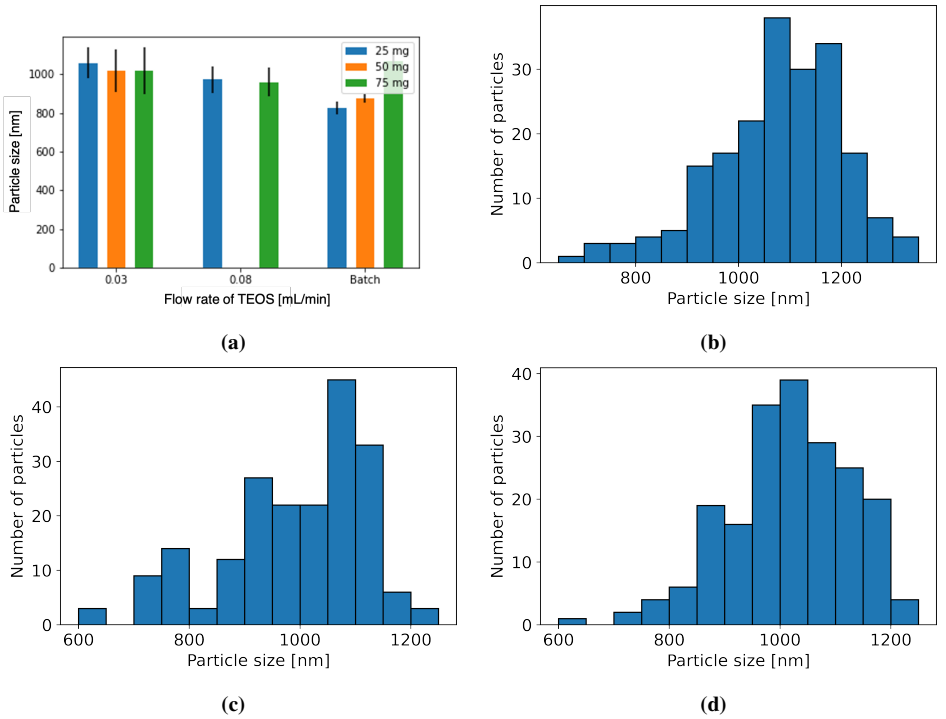

Figure 6.23: **(a)** Particle sizes for experiments performed using different masses of cIONPs, PSDs for **(b)** 25 mg, **(c)** 50 mg and **(d)** 75 mg of cIONPs with use of isopropanol and flow rates of 0.1 mL/min and 0.008 mL/min for ammonium hydroxide and TEOS respectively.

VSM measurements were performed for I-25*0.1-L, I-75*0.1-L, I-25*0.1-H, and I-75*0.1-H to see if the mass of cIONPs affected the magnetic properties of the products. Figure 6.24 shows the hysteresis loop for the samples. As can be seen in Figure 6.24, higher moments are obtained using 75 mg cIONPs. This means that the final products contain more cIONPs when a higher mass is used.

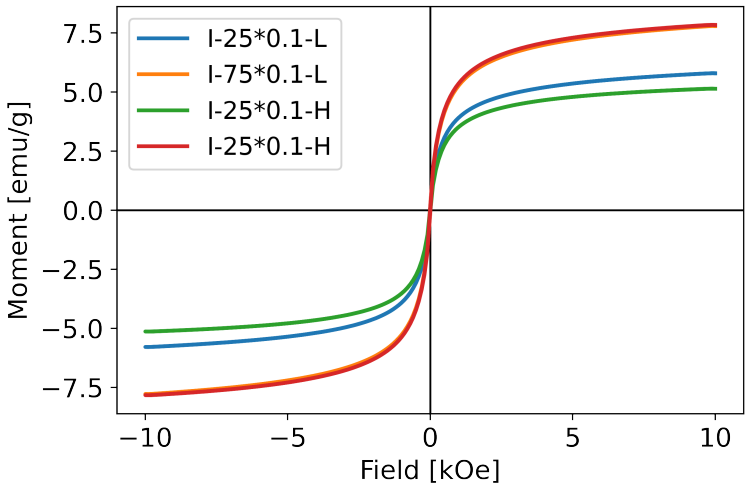

Figure 6.24: Magnetic properties of ScIONPs obtained using different cIONPs masses.

6.2.5.2 Effect of TEOS Flow Rate

In literature, the flow rate of TEOS is reported to be an essential parameter in the modified Stöber method. In this study, a total amount of 2 mL of TEOS was used for all experiments, however, using two different flow rates, 0.03 mL/min and 0.08 mL/min, making the amount being injected over a period of 60 min and 25 min, respectively.

Firstly, the amount of TEOS needs to be considered. As reported in the literature, the concentration of TEOS must be limited to avoid agglomerations that result in irregularly shaped particles. A high concentration of TEOS may lead to disturbance in the nucleation and growth steps [29]. It is thus vital to find the balance between the reaction conditions and the TEOS concentration. By using a semi-batch set-up, an appropriate balance can be achieved by introducing the TEOS over time. To avoid any further nucleation, the concentration of TEOS, and hence free silicic acid, can be kept low enough, and a high degree of monodispersity may be achieved.

For the experiments where the same parameters are used, except changing the flow rate between 0.03 mL/min and 0.08 mL/min, a general trend is that the flow rate of 0.08 mL/min gave smaller particles than the flow rate of 0.03 mL/min. Figure 6.26 shows the effect of TEOS flow rate on the particle sizes, including the standard deviations, for experiments where all remaining parameters are kept constant. The green bars, where the rate of TEOS is 0, are the corresponding sizes obtained by Ali [4] in the batch experiments. As shown in Figure 6.26, the particle sizes tend to decrease with the increasing flow rate of TEOS, except for I-50*0.054-L and I-50*0.054-H. This trend coincides with the findings of Kim and Kim [42] and Luo et al. [54]. However, it should be noted that in this study, both ammonium hydroxide and TEOS are added over time, while in the studies of Kim and Kim

and Luo et al., only TEOS was added over time. In this experiment, it is thus essential to find a balance between the two flow rates.

When TEOS is hydrolyzed, there are two possible outcomes as described in 4.2, it may either condense on already existing nuclei or form new nuclei. If condensation is the case, growth will consequently occur, leading to particles of bigger sizes. However, if nucleation occurs, smaller particles will be the outcome. It is thus expected that if a too high flow rate of TEOS is used, the formation of new nuclei is favored as there will be an excess of hydrolyzed TEOS. The concentration will hence be above the critical concentration for nucleation. When a slower flow rate is used, the concentration will be below the critical concentration, and growth will give bigger particles.

Giesche [29] states that the flow rate of TEOS is essential and needs to be considered as a result of the ammonium hydroxide concentration. He showed that the particle growth rate is slow at low ammonium hydroxide concentration, thus needing a slow addition of TEOS. He states that when TEOS is added too fast, the concentration of silanol monomers constantly increases and exceeds the self-nucleation concentration, resulting in the formation a new particle population.

The standard deviations in these experiments reveal that the higher flow rate of TEOS tends to produce particles with a higher degree of monodispersity. The particle size distributions for E-50*0.054-L and E-50*0.054-H are shown in Figure 6.25, whereas the distribution for E-50*0.054-H, i.e., the higher flow rate, is more narrow.

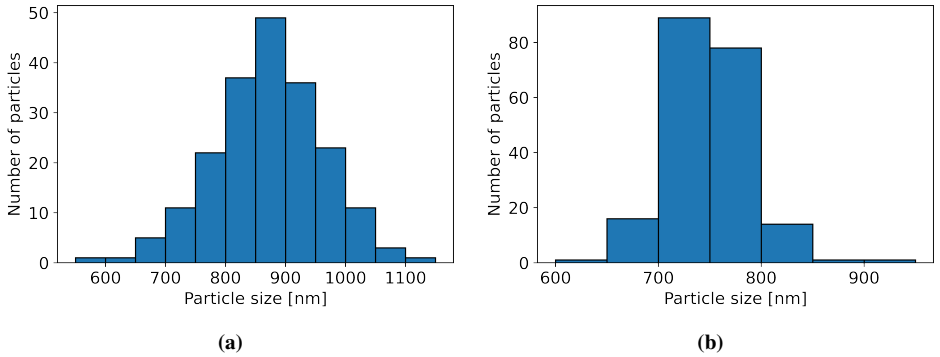

Figure 6.25: Particle size distribution for (a) E-50*0.0054-L and (b) E-50*0.0054-H.

It is expected that an even higher flow rate of TEOS would give even smaller particles with even lower standard deviations, however, a too high flow rate of TEOS will result in a high concentration of silicic acid units. The concentration might reach the critical limit for self nucleation, which would disturb the product's monodispersity.

Regarding the morphologies obtained in these experiments where the TEOS flow rate is varied, the flow rate does not have any effect. In all the pairs of experiments in Figure 6.26, the same morphologies are observed, either if it is spheres, incompletely fused particles,

or agglomerates. This is also the case for the experiments where the slowest flow rate of ammonium hydroxide is used, and there are no spherical particles observed. Varying the flow rate of TEOS in these cases does not reveal any different morphologies as only irregular particles are observed.

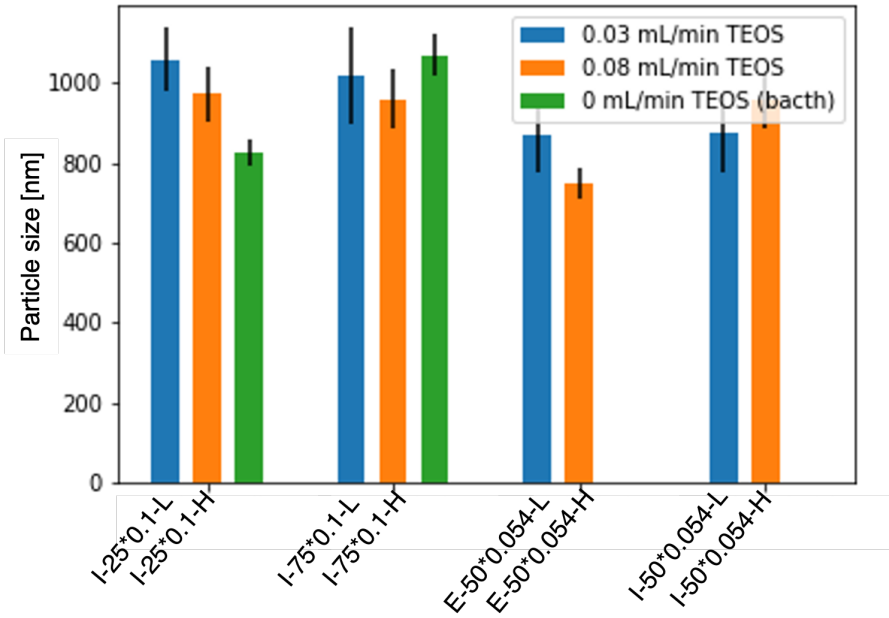

Figure 6.26: Particle sizes as a result of different flow rates of TEOS.

6.2.5.3 Overall Effects of Reaction Parameters

Looking at the results obtained from the experimental design, as a big picture, many factors are influencing the particle sizes and morphologies. Especially for the morphology, the flow rate and thus the concentration of ammonium hydroxide are essential factors. Also, the use of solvent had a significant influence on morphology. The mass of cIONPs appeared to affect the morphology when lower masses were used. However, at higher masses, there was no significant effect on the morphology or particle size. For the particle sizes, ammonium hydroxide and TEOS flow rate seemed to be the most significant factors. However, this is only valid for the spherical particles, as the irregular-shaped particles' sizes could not be measured.

6.2.6 Statistical Analysis

For the experiments where the final particle sizes were measurable, the mean sizes were fitted into an effective screening model using JMP. Root mean square error is then used to find the correlation between the predicted sizes and the actual sizes of the particles. The two different solvents, the mass of cIONPs, the flow rate of ammonium hydroxide, and the flow rate of TEOS, were used as input parameters. The fitted model is shown in Figure 6.27. For each of the input parameters, the probability value is calculated, giving an indication of the significance of the different parameters. This model states that the most significant factor in these experiments is the ammonium hydroxide flow rate with a p-value of 0.028. The solvent is the second most significant factor, then comes the mass of cIONPs and TEOS flow rate, which is the least significant factor. The R^2 was calculated to be 0.84.

It needs to be emphasized that these results are based on a set of experiments where, for some combinations of reaction parameters, the results could not be fitted in the model because the size could not measure. For example, with ethanol, many experiments gave particles of irregular shapes, which in order affects the model created by JMP as it is excluded from the model fit.

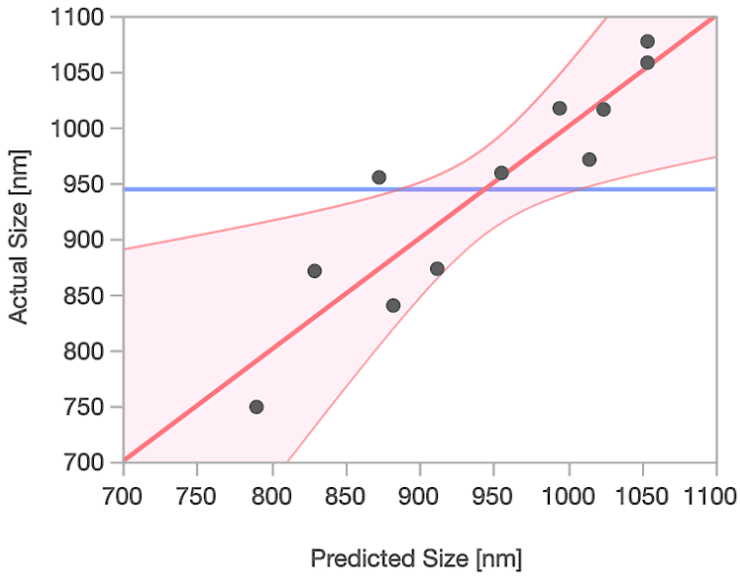

Figure 6.27: Statistical model fitting performed in JMP.

6.2.7 Magnetic Properties

As mentioned earlier, the uniqueness of IONPs lies mainly in their superparamagnetic properties. Hence, it is of the utmost importance to maintain these properties after functionalization so that the particles still meet the criteria for various applications. The magnetic properties of the silica coated particles were measured using VSM. While some hysteresis loops are already presented under different reaction parameters, this is a summary of all the VSM measurements. VSM measurements were only performed for samples where spheres, incompletely fused particles and agglomerates were observed. In Figure 6.28 the hysteresis loops for the semi-batch experiments are shown. As can be seen in the figure, the magnetization varies from 4 emu/g to 8 emu/g. This is very low compared to the magnetization of the bare cIONPs particles, where the magnetization was around 60 emu/g. A decrease is expected as the particles are coated with a non-magnetic shell of silica. However, it is desired to achieve final particles with higher moments.

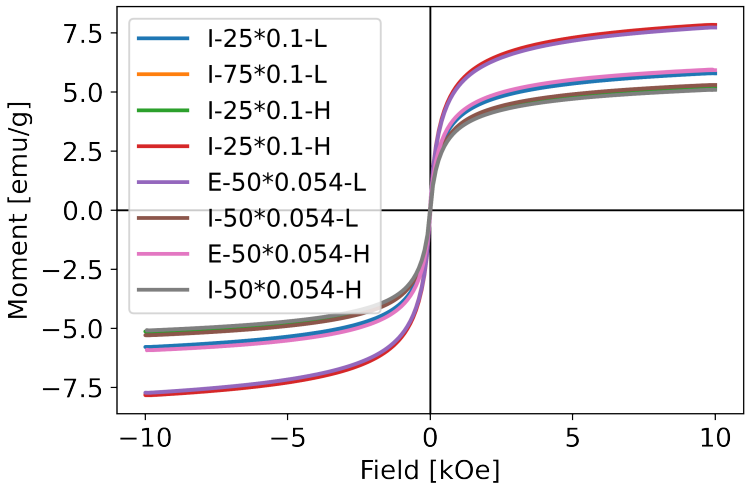

Figure 6.28: Hysteresis loops for silica coated cIONPs.

Taking the parameters used in the different experiments into consideration, there are not many trends that can be recognized. Except for the use of different masses of cIONPs as presented in section 6.2.5.1.

Chapter 7

Final Remarks

7.1 Conclusions

In this study, a modified Stöber method for the silanization of iron oxide nanoparticles (IONPs) using a semi-batch set up has been investigated. The aim was to study how the semi-batch set up differs from a batch set up and investigate if the addition of reactants over time can help tune the particle sizes, size distributions, and morphologies.

The reaction parameters varied in this set of experiments were the flow rate of ammonium hydroxide, the flow rate of TEOS, the nature of the solvent, and the mass of IONPs. A custom design of experiments was made using JMP. It has been proven that the combinations of different reaction parameters are essential for the final result and especially the morphology of the particles. Particles have successfully been synthesized in sizes ranging from 749$\pm$38 nm to 1058$\pm$81 nm. The different morphologies obtained in this study were spherical particles, incompletely fused particles, agglomerates, and irregularly shaped particles.

The nature of solvent has been demonstrated to be essential for the morphologies obtain. While isopropanol in most cases resulted in spherical particles, ethanol often gave irregular particles. However, for the cases where spherical particles were obtained in ethanol, smaller particle sizes were achieved compared to isopropanol. The mass of IONPs was important for the final morphology. When low masses of IONPs were used, 25 mg, incompletely fused particles were observed. However, when higher masses were used, 50 mg and 75 mg, spherical particles were obtained. When spherical particles were obtained, the mass of IONPs did not have a significant effect on the particle size. However, VSM measurements showed that higher magnetization was obtained using bigger masses of IONPs. For ammonium hydroxide, firstly, the total volume added was important. At low molarities of ammonium hydroxide, only irregular shaped particles were observed. For higher molar-

ities, all morphologies were observed. For experiments using fixed volumes of ammonium hydroxide, lower flow rates gave smaller particles with narrower size distributions. The flow rate of TEOS was also significant, giving smaller particles at higher flow rates. The TEOS flow rate did not have a significant effect on the particle morphology.

Overall, it has been shown that different reaction parameters affect particle sizes and morphologies. While some parameters affect both the size and morphology, other parameters only significantly affect the particle size or the morphology. The particle sizes and morphologies can hence be tuned by varying the reaction conditions. The smallest obtained spherical particles in this study were achieved using ethanol as the solvent, 50 mg of IONPs, a middle flow rate of ammonium hydroxide, and a high flow rate of TEOS. However, more studies will be necessary to find the optimum conditions for these experiments.

7.2 Future Work

Future work should focus on obtaining a higher number of spherical particles and less irregular shaped particles. Spherical particles are successfully synthesized in this study, however, irregular particles are observed for all reaction conditions. It would be interesting to study how the pH varies over time. As shown in this study, the total volume and the flow rate of ammonium hydroxide are important parameters affecting particle sizes. By doing pH measurements during the reaction, the growth of particles can be further investigated and might open for better control of the final particles' size. The ammonium hydroxide could be introduced over an even extended period of time.

Another critical aspect to work on, is obtaining particles with higher magnetization values. Higher magnetization values might be necessary for many applications, so studies focusing on achieving a higher ratio of iron to silica will thus be essential. In this study, a fixed volume of TEOS is used; varying this amount would be interesting to see if the silicon content can be tuned. Using bigger masses of IONPs might also be a good idea.

Overall, it will be essential to investigate how the different reaction parameters act in synergy, focusing on obtaining less irregular particles and secondary population and higher magnetization values. For this set of experiments, it would also be recommended to use a full factorial design, as in this study, where a custom design was used, a lot of extra experiments had to be added.

Bibliography

[1]

[2] A.O. Adeyeye and G. Shimon. Chapter 1 - growth and characterization of magnetic thin film and nanostructures. 5:1–41, 2015.

[3] Attarad Ali, Hira Zafar, M. Zia, I. ul haq, A. Phull, J. S. Ali, and Altaf Hussain. Synthesis, characterization, applications, and challenges of iron oxide nanoparticles. *Nanotechnology, Science and Applications*, 9:49 – 67, 2016.

[4] Zeeshan Ali. Insights into growth mechanism, control of particle size and particle size distribution of silica coated iron oxide nanoparticles. *Deparment of Chemical Engineering, Norwegian University of Science and Technology*, 2020.

[5] Jens-Petter Andreassen and Alison Emslie Lewis. *Classical and Nonclassical Theories of Crystal Growth*, pages 137–154. Springer International Publishing, Cham, 2017.

[6] Monica Araya-Farias, Szymon Dziomba, and N. Thuy Tran. Chapter 3 - microfluidic strategies for extraction and preconcentration of proteins and peptides. In Chaudhery Mustansar Hussain, editor, *Handbook on Miniaturization in Analytical Chemistry*, pages 35–75. Elsevier, 2020.

[7] Marzban Arefi, Maryam Kazemi, Ramin Mostafalu, Mohammad Satari, and Akbar Heydari. Citric acid stabilized on the surface of magnetic nanoparticles as an efficient and recyclable catalyst for transamidation of carboxamides, phthalimide, urea and thiourea with amines under neat conditions. *Journal of the Iranian Chemical Society*, 16, 10 2018.

[8] Lucia Babes, Benoit Denizot, Gisèle Tanguy, Jean Jacques Le Jeune, and Pierre Jallet. Synthesis of iron oxide nanoparticles used as mri contrast agents: A parametric study. *Journal of Colloid and Interface Science*, 212(2):474–482, 1999.

[9] Lydia Bahrig, Stephen Hickey, and Alexander Eychmüller. Mesocrystalline materials and the involvement of oriented attachment – a review. *CrystEngComm*, 16, 09 2014.

[10] F. Baillon, F. Espitalier, C. Cogné, R. Peczalski, and O. Louisnard. 28 - crystallization and freezing processes assisted by power ultrasound. In Juan A. Gallego-Juárez and Karl F. Graff, editors, *Power Ultrasonics*, pages 845–874. Woodhead Publishing, Oxford, 2015.

[11] Sulalit Bandyopadhyay. *Fabrication and Application of Nanomaterials*. McGraw Hill Professional, 2019.

[12] Carlos Bárcena, Amandeep K. Sra, and Jinming Gao. *Applications of Magnetic Nanoparticles in Biomedicine*, pages 591–626. Springer US, Boston, MA, 2009.

[13] Atul H. Bari, Rajashri B. Jundale, and Amol.A. Kulkarni. Understanding the role of solvent properties on reaction kinetics for synthesis of silica nanoparticles. *Chemical Engineering Journal*, 398:125427, 2020.

[14] R. Becker and W. Döring. Kinetische Behandlung der Keimbildung in übersättigten Dämpfen. *Annalen der Physik*, 416(8):719–752, January 1935.

[15] Wolfgang Beckmann. *Mechanisms of Crystallization*, chapter 2, pages 7–33. John Wiley & Sons, Ltd.

[16] I.N Bhattacharya, J.K Pradhan, P.K Gochhayat, and S.C Das. Factors controlling precipitation of finer size alumina trihydrate. *International Journal of Mineral Processing*, 65(2):109–124, 2002.

[17] G.H. Bogush, M.A. Tracy, and C.F. Zukoski. Preparation of monodisperse silica particles: Control of size and mass fraction. *Journal of Non-Crystalline Solids*, 104(1):95–106, 1988.

[18] G.H Bogush and C.F Zukoski. Uniform silica particle precipitation: An aggregative growth model. *Journal of Colloid and Interface Science*, 142(1):19–34, 1991.

[19] R. Boistelle and J.P. Astier. Crystallization mechanisms in solution. *Journal of Crystal Growth*, 90(1):14–30, 1988.

[20] Chin Fei Chee, Bey Fen Leo, and Chin Wei Lai. 37 - superparamagnetic iron oxide nanoparticles for drug delivery. In Inamuddin, Abdullah M. Asiri, and Ali Mohammad, editors, *Applications of Nanocomposite Materials in Drug Delivery*, Woodhead Publishing Series in Biomaterials, pages 861–903. Woodhead Publishing, 2018.

[21] Elham Cheraghipour, Sirus Javadpour, and Ali Mehdizadeh. Citrate capped superparamagnetic iron oxide nanoparticles used for hyperthermia therapy. *Journal of Biomedical Science and Engineering*, 05:715–719, 01 2012.

[22] Elham Cheraghipour, Sirus Javadpour, and Ali Mehdizadeh. Citrate capped superparamagnetic iron oxide nanoparticles used for hyperthermia therapy. *Journal of Biomedical Science and Engineering*, 05:715–719, 01 2012.

[23] Peter Crafts. Chapter 2 - the role of solubility modeling and crystallization in the design of active pharmaceutical ingredients. In Ka M. Ng, Rafiqul Gani, and Kim Dam-Johansen, editors, *Chemical Product Design: Toward a Perspective Through Case Studies*, volume 23 of *Computer Aided Chemical Engineering*, pages 23–85. Elsevier, 2007.

[24] Hongtao Cui, Yongmei Feng, Wanzhong Ren, Tao Zeng, Hongying Lv, and Yanfei Pan. Strategies of large scale synthesis of monodisperse nanoparticles. *Recent Patents on Nanotechnology*, 3:32–41, 02 2009.

[25] Mohammed Dheyab, Azlan Abdul Aziz, Mahmood Jameel, Osama abu noqta, Pegah Moradi, and Baharak Mehrdel. Simple rapid stabilization method through citric acid modification for magnetite nanoparticles. *Scientific Reports*, 07 2020.

[26] Mohamed M. Fathy, Heba M. Fahmy, Omnia A. Saad, and Wael M. Elshemey. Silica-coated iron oxide nanoparticles as a novel nano-radiosensitizer for electron therapy. *Life Sciences*, 234:116756, 2019.

[27] J. Frenkel. A general theory of heterophase fluctuations and pretransition phenomena. *The Journal of Chemical Physics*, 7(7):538–547, 1939.

[28] Pramila P. Ghimire and Mietek Jaroniec. Renaissance of stöber method for synthesis of colloidal particles: New developments and opportunities. *Journal of Colloid and Interface Science*, 584:838–865, 2021.

[29] Herbert Giesche. Synthesis of monodispersed silica powders ii. controlled growth reaction and continuous production process. *Journal of the European Ceramic Society*, 14(3):205–214, 1994.

[30] Joseph Govan and Yurii K. Gunko. Recent advances in the application of magnetic nanoparticles as a support for homogeneous catalysts. *Nanomaterials*, 4(2):222–241, 2014.

[31] Ying Wang Guozhong Cao. *Nanostructures and Nanomaterials. Synthesis, Properties, and Applications*. World Scientific, 2010.

[32] Maribel G. Guzmán, Jean Dille, and Stephan Godet. Synthesis of silver nanoparticles by chemical reduction method and their antibacterial activity. *International Journal of Materials and Metallurgical Engineering*, 2(7):91 – 98, 2008.

[33] Sašo Gyergyek, Miha Drofenik, and Darko Makovec. Oleic-acid-coated cofe2o4 nanoparticles synthesized by co-precipitation and hydrothermal synthesis. *Materials Chemistry and Physics*, 133(1):515–522, 2012.

[34] Yandong Han, Ziyang Lu, Zhaogang Teng, Jinglun Liang, Zilong Guo, Dayang Wang, Ming-Yong Han, and Wensheng Yang. Unraveling the growth mechanism of silica particles in the stöber method: In situ seeded growth model. *Langmuir*, 33(23):5879–5890, 2017. PMID: 28514596.

[35] Michael T. Harris, Ronald R. Brunson, and Charles H. Byers. The base-catalyzed hydrolysis and condensation reactions of dilute and concentrated teos solutions. *Journal of Non-Crystalline Solids*, 121(1):397–403, 1990. Proceedings of the Fifth International Workshop on Glasses and Ceramics from Gels.

[36] D.R. Hristov, E. Mahon, and K.A. Dawson. Controlling aqueous silica nanoparticle synthesis in the 10-100 nm range. *Chemical Communications*, 51(98):17420–17423, 2015. cited By 15.

[37] Chia Chin Hua, Sarani Zakaria, R Farahiyan, Liew Tze Khong, et al. Size-controlled synthesis and characterization of fe. *Sains Malaysiana*, 37(4):389–394, 2008.

[38] SAS Institute Inc. Custom Designs. Construct Designs That Meet Your Needs. `https://www.jmp.com/support/help/en/16.0/index.shtml#page/jmp/custom-designs.shtml`. [Online; accessed 20.05.2021].

[39] Prasad Govindrao Jamkhande, Namrata W. Ghule, Abdul Haque Bamer, and Mohan G. Kalaskar. Metal nanoparticles synthesis: An overview on methods of preparation, advantages and disadvantages, and applications. *Journal of Drug Delivery Science and Technology*, 53:101174, 2019.

[40] S. Karthika, T. K. Radhakrishnan, and P. Kalaichelvi. A review of classical and nonclassical nucleation theories. *Crystal Growth & Design*, 16(11):6663–6681, 2016.

[41] Sanjay Kashyap, Taylor J. Woehl, Xunpei Liu, Surya K. Mallapragada, and Tanya Prozorov. Nucleation of iron oxide nanoparticles mediated by mms6 protein in situ. *ACS Nano*, 8(9):9097–9106, 2014. PMID: 25162493.

[42] Ki Kim and Hee Taik Kim. Formation of silica nanoparticles by hydrolysis of teos using a mixed semi-batch/batch method. *Journal of Sol-Gel Science and Technology*, 25:183–189, 12 2002.

[43] Barbara Korzeniowska, Robert Nooney, Dorota Wencel, and Colette Mcdonagh. Silica nanoparticles for cell imaging and intracellular sensing. *Nanotechnology*, 24:442002, 10 2013.

[44] Ruslan Kostov. Crystals: Growth, morphology and perfection: by i. sunagawa. *Canadian Mineralogist - CAN MINERALOG*, 43:1127–1128, 06 2005.

[45] Roman Krahne, Giovanni Morello, Albert Figuerola, Chandramohan George, Sasanka Deka, and Liberato Manna. Physical properties of elongated inorganic nanoparticles. *Physics Reports*, 501(3):75–221, 2011.

[46] Alec P. LaGrow, Maximilian O. Besenhard, Aden Hodzic, Andreas Sergides, Lara K. Bogart, Asterios Gavriilidis, and Nguyen Thi Kim Thanh. Unravelling the growth mechanism of the co-precipitation of iron oxide nanoparticles with the aid of synchrotron x-ray diffraction in solution. *Nanoscale*, 11:6620–6628, 2019.

[47] Ramnath Lakshmanan, Chuka Okoli, Magali Boutonnet, Sven Järås, and Gunaratna K. Rajarao. Effect of magnetic iron oxide nanoparticles in surface water treatment: Trace minerals and microbes. *Bioresource Technology*, 129:612–615, 2013.

[48] V.K. Lamer and R.H. Dinegar. Theory, production and mechanism of formation of monodispersed hydrosols. *Journal of the American Chemical Society*, 72(11):4847–4854, 1950.

[49] Dae Ho Lee, Sung Eun Han, and Dong Kang. Size change of silica nanoparticles induced by non-alcoholic solvent addition during sol–gel reaction. *Journal of Sol-Gel Science and Technology*, 74:78–83, 04 2014.

[50] Suoyuan Lian, Enbo Wang, Zhenhui Kang, Yunpeng Bai, Lei Gao, Min Jiang, Changwen Hu, and Lin Xu. Synthesis of magnetite nanorods and porous hematite nanorods. *Solid State Communications*, 129(8):485–490, 2004.

[51] Cheng-Han Lin, Jen-Hsuan Chang, Yi-Qi Yeh, Si-Han Wu, Yi-Hsin Liu, and Chung-Yuan Mou. Formation of hollow silica nanospheres by reverse microemulsion. *Nanoscale*, 7:9614–9626, 2015.

[52] An-Hui Lu, E.L. Salabas, and Ferdi Schüth. Magnetic nanoparticles: Synthesis, protection, functionalization, and application. *Angewandte Chemie International Edition*, 46(8):1222–1244, 2007.

[53] Ziyang Lu, Jie Dai, Xiangning Song, Gang Wang, and Wensheng Yang. Facile synthesis of fe3o4/sio2 composite nanoparticles from primary silica particles. *Colloids and Surfaces A: Physicochemical and Engineering Aspects*, 317(1):450–456, 2008.

[54] Xiongfang Luo, Jing Dong, Lulu Zhang, Jinmei Du, Hongbo Wang, and Weidong Gao. Preparation of silica micro spheres via a semibatch sol–gel method. *Journal of Sol-Gel Science and Technology*, 81:1–9, 03 2017.

[55] Dongling Ma, Jingwen Guan, , Stéphane Dénommée, Gary Enright, Teodor Veres, and Benoit Simard. Multifunctional nano-architecture for biomedical applications. *Chemistry of Materials*, 18(7):1920–1927, 2006.

[56] Mahnaz Mahdavi, Mansor Ahmad, Md Jelas Haron, Farideh Namvar, Behzad Nadi, Mohamad Rahman, and Jamileh Amin. Synthesis, surface modification and characterisation of biocompatible magnetic iron oxide nanoparticles for biomedical applications. *Molecules (Basel, Switzerland)*, 18:7533–7548, 06 2013.

[57] Vahak Marghussian. 4 - magnetic properties of nano-glass ceramics. In Vahak Marghussian, editor, *Nano-Glass Ceramics*, pages 181 – 223. William Andrew Publishing, Oxford, 2015.

[58] Maria Cristina Mascolo, Yongbing Pei, and Terry Ring. Room temperature co-precipitation synthesis of magnetite nanoparticles in a large ph window with different bases. *Materials*, 6, 11 2013.

[59] Rene Massart. Preparation of aqueous magnetic liquids in alkaline and acidic media. ieee transactions on magnetics. 17(2):1247–1248, 1981.

[60] T Matsoukas and Erdogan Gulari. Dynamics of growth of silica particles from ammonia-catalyzed hydrolysis of tetra-ethyl-orthosilicate. *Journal of Colloid and Interface Science*, 124(1):252–261, 1988.

[61] E. Mine, D. Nagao, Y. Kobayashi, and M. Konno. Solvent effects on particle formation in hydrolysis of tetraethyl orthosilicate. *Journal of Sol-Gel Science and Technology*, 35:197–201, 2005.

[62] Giulia Mirabello, Jos J. M. Lenders, and Nico A. J. M. Sommerdijk. Bioinspired synthesis of magnetite nanoparticles. *Chem. Soc. Rev.*, 45:5085–5106, 2016.

[63] J. W. Mullin. *Crystallization (4th ed., pp. XV, 594)*. Butterworth-Heinemann., 2001.

[64] nanoScience Instruments. Magnetic Beads. `https://www.antibodies-online.com/resources/17/5035/magnetic-beads/`. [Online; accessed 23.10.2020].

[65] nanoScience Instruments. Scanning Electron Microscopy. `https://www.nanoscience.com/techniques/scanning-electron-microscopy/`. [Online; accessed 14.11.2020].

[66] Arne Erik Nielsen and Jens M. Toft. Electrolyte crystal growth kinetics. *Journal of Crystal Growth*, 67(2):278–288, 1984.

[67] Saumya Nigam, K.C. Barick, and D. Bahadur. Development of citrate-stabilized fe3o4 nanoparticles: Conjugation and release of doxorubicin for therapeutic applications. *Journal of Magnetism and Magnetic Materials*, 323(2):237–243, 2011.

[68] Norwegian University of Science and Technology. NTNU COVID-19 test. `https://www.ntnu.edu/ntnu-covid-19-test`. [Online; accessed 05.05.21].

[69] Chuka Okoli, Margarita Sanchez-Dominguez, Magali Boutonnet, Sven Järås, Concepción Civera, Conxita Solans, and Gunaratna Rajarao Kuttuva. Comparison and functionalization study of microemulsion-prepared magnetic iron oxide nanoparticles. *Langmuir*, 28(22):8479–8485, 2012. PMID: 22578053.

[70] Malvern Panalytical. Dynamic Light Scattering (DLS). `https://www.malvernpanalytical.com/en/products/technology/light-scattering/dynamic-light-scattering`. [Online; accessed 05.03.2020].

[71] K. Petcharoen and A. Sirivat. Synthesis and characterization of magnetite nanoparticles via the chemical co-precipitation method. *Materials Science and Engineering: B*, 177(5):421–427, 2012.

[72] Xuan-Hung Pham, Eunil Hahm, Hyung-Mo Kim, Byung Sung Son, Ahla Jo, Jaehyun An, Tuong An Tran Thi, Dinh Quan Nguyen, and Bong-Hyun Jun. Silica-coated magnetic iron oxide nanoparticles grafted onto graphene oxide for protein isolation. *Nanomaterials*, 10(1), 2020.

[73] Zeena S. Pillai and Prashant V. Kamat. What factors control the size and shape of silver nanoparticles in the citrate ion reduction method? *The Journal of Physical Chemistry B*, 108(3):945–951, 2004.

[74] Jörg Polte. Fundamental growth principles of colloidal metal nanoparticles – a new perspective. *CrystEngComm*, 17:6809–6830, 2015.

[75] polymerdatabase.com. THERMODYNAMICS OF HOMOGENEOUS NUCLEATION. `https://polymerdatabase.com/polymer%20physics/Spherulites.html`. [Online; accessed 23.04.2021].

[76] D. Pouliquen, J.J. Le Jeune, R. Perdrisot, A. Ermias, and P. Jallet. Iron oxide nanoparticles for use as an mri contrast agent: Pharmacokinetics and metabolism. *Magnetic Resonance Imaging*, 9(3):275–283, 1991.

[77] Michela Puddu, Daniela Paunescu, Wendelin J. Stark, and Robert N. Grass. Magnetically recoverable, thermostable, hydrophobic dna/silica encapsulates and their application as invisible oil tags. *ACS Nano*, 8(3):2677–2685, 2014. PMID: 24568212.

[78] P. Pusey. The effect of polydispersity on the crystallization of hard spherical colloids. *Journal de Physique*, 48(5):709–712.

[79] Dongming Qi, Chao Lin, Hongting Zhao, Hu Liu, and Ting Lü. Size regulation and prediction of the sio2 nanoparticles prepared via stöber process. *Journal of Dispersion Science and Technology*, 38(1):70–74, 2017.

[80] Rasoul Rahimnia, Zeinab Salehi, Mehdi Ardestani, and Hamid Doosthoseini. Spion conjugated curcumin nano-imaging probe: Synthesis and bio-physical evaluation. *Iranian journal of pharmaceutical research (IJPR)*, 01 2018.

[81] Wegdan Ramadan, Marwa Karim, Beatrice Hannoyer, and Shanta Saha. Effect of ph on the structural and magnetic properties of magnetite nanoparticles synthesised by co-precipitation. *Advanced Materials Research*, 324:129–132, 08 2012.

[82] Ren G.and Su H.and Wang S. The combined method to synthesis silica nanoparticle by stöber process. *J Sol-Gel Sci Technol*, 96:108–120, 2020.

[83] Yudhisthira Sahoo, Alireza Goodarzi, Mark T. Swihart, Tymish Y. Ohulchanskyy, Navjot Kaur, Edward P. Furlani, and Paras N. Prasad. Aqueous ferrofluid of magnetite nanoparticles: fluorescence labeling and magnetophoretic control. *The Journal of Physical Chemistry B*, 109(9):3879–3885, 2005. PMID: 16851439.

[84] M A Sharaf. Preparation of spherical nanoparticles: Stober silica. *Journal of American Science*, 6:985–989, 01 2010.

[85] Geetu Sharma and Pethaiyan Jeevanandam. Synthesis of self-assembled prismatic iron oxide nanoparticles by a novel thermal decomposition route. *RSC Adv.*, 3:189–200, 2013.

[86] Abeer Jabra Shnoudeh, Islam Hamad, Ruwaida W. Abdo, Lana Qadumii, Abdulmutallab Yousef Jaber, Hiba Salim Surchi, and Shahd Z. Alkelany. Chapter 15 - synthesis, characterization, and applications of metal nanoparticles. In Rakesh K. Tekade, editor, *Biomaterials and Bionanotechnology*, Advances in Pharmaceutical Product Development and Research, pages 527 – 612. Academic Press, 2019.

[87] Anthony Singer, Zein Barakat, Subhra Mohapatra, and Shyam S. Mohapatra. Chapter 13 - nanoscale drug-delivery systems: In vitro and in vivo characterization. In Shyam S. Mohapatra, Shivendu Ranjan, Nandita Dasgupta, Raghvendra Kumar Mishra, and Sabu Thomas, editors, *Nanocarriers for Drug Delivery*, Micro and Nano Technologies, pages 395–419. Elsevier, 2019.

[88] Stefaan J. H. Soenen, Uwe Himmelreich, Nele Nuytten, Thomas R. Pisanic II, Aldo Ferrari, and Marcel De Cuyper. Intracellular nanoparticle coating stability determines nanoparticle diagnostics efficacy and cell functionality. *Small*, 6(19):2136–2145, 2010.

[89] James G. Speight. Chapter 3 - industrial organic chemistry. In James G. Speight, editor, *Environmental Organic Chemistry for Engineers*, pages 87–151. Butterworth-Heinemann, 2017.

[90] Srećko Stopić, Felix Wenz, Tatjana-Volkov Husovic, and Bernd Friedrich. Synthesis of silica particles using ultrasonic spray pyrolysis method. *Metals*, 11:463, 03 2021.

[91] Werner Stöber, Arthur Fink, and Ernst Bohn. Controlled growth of monodisperse silica spheres in the micron size range. *Journal of Colloid and Interface Science*, 26(1):62 – 69, 1968.

[92] Tadao Sugimoto. Underlying mechanisms in size control of uniform nanoparticles. *Journal of Colloid and Interface Science*, 309(1):106–118, 2007. Matijevic Festschrift.

[93] Jing Sun, Shaobing Zhou, Peng Hou, Yuan Yang, Jie Weng, Xiaohong Li, and Mingyuan Li. Synthesis and characterization of biocompatible fe3o4 nanoparticles. *Journal of biomedical materials research. Part A*, 80:333–41, 02 2007.

[94] Z.X. Tang, S. Nafis, C.M. Sorensen, G.C. Hadjipanayis, and K.J. Klabunde. Magnetic properties of aerosol synthesized iron oxide particles. *Journal of Magnetism and Magnetic Materials*, 80(2):285–289, 1989.

[95] Pedro Tartaj, Maria del Puerto Morales, Sabino Veintemillas-Verdaguer, Teresita Gonzalez-Carreño, and C. Serna. chapter 5 synthesis, properties and biomedical applications of magnetic nanoparticles. *Handbook of Magnetic Materials*, 16:403–482, 12 2006.

[96] Dan V. Goia and Egon Matijević. Preparation of monodispersed metal particles. *New J. Chem.*, 22:1203–1215, 1998.

[97] A.K. Van Helden, J.W. Jansen, and A. Vrij. Preparation and characterization of spherical monodisperse silica dispersions in nonaqueous solvents. *Journal of Colloid and Interface Science*, 81(2):354–368, 1981.

[98] M. Volmer and A. Weber. Keimbildung in übersättigten gebilden. *Zeitschrift für Physikalische Chemie*, 119U(1):277–301, 1926.

[99] Jiakun Xu, Jingjing Sun, Yuejun Wang, Jun Sheng, Fang Wang, and Mi Sun. Application of iron magnetic nanoparticles in protein immobilization. *Molecules*, 19(8):11465–11486, 2014.

[100] Djamal Zerrouki, Benjamin Rotenberg, Sébastien Abramson, Jean Baudry, Cécile Goubault, Fernando Leal-Calderon, Dave J. Pine, and Jérome Bibette. Preparation of doublet, triangular, and tetrahedral colloidal clusters by controlled emulsification. *Langmuir*, 22(1):57–62, 2006. PMID: 16378400.

[101] Hong-wang Zhang, Yi Liu, and Shou-heng Sun. Synthesis and assembly of magnetic nanoparticles for information and energy storage applications. *Frontiers of Physics in China*, 5:347–356, 12 2010.

[102] Nan Zhu, Haining Ji, Peng Yu, Jiaqi Niu, M. U. Farooq, M. Waseem Akram, I. O. Udego, Handong Li, and Xiaobin Niu. Surface modification of magnetic iron oxide nanoparticles. *Nanomaterials*, 8(10), 2018.

Appendix A

Protocols

A.1 Citrate Coated Iron Oxide Nanoparticles

1. Weigh 1.732 g $FeCl_2 \cdot H_2O$ in a weighing boat.
2. Crush $FeCl_3 \cdot H_2O$ in a mortar using a pestle to fine powder.
3. Weigh 4.44 g of the fine powder of $FeCl_3 \cdot {}_6H_2O$ in a weighing boat.
4. Add both salts into the reactor and dissolve in 80 mL MQ water.
5. Clean a magnetic stirrer bar with MQ water and place it in the reactor.
6. Place the reactor on a magnetic stirrer at 1000 rpm.
7. Connect the condenser and gas line using nitrogen gas.
8. Connect the Julabo water bath.
9. Heat the water bath to 70 °C and maintain for 30 minutes.
10. Add 20 mL of 25 wt% NH_4OH to the reactor.
11. Maintain the temperature at 70 °C for another 30 minutes.
12. Add 4 mL aqueous solution of citric acid (0.5 g/mL).
13. Slowly increase the temperature to 90 °C and maintain for 60 minutes.
14. Stop the heating and cool to solution to room temperature.
15. Transfer the solution to a 50 mL centrifuge tube in multiple steps and separate the magnetic particles in each step using a permanent magnet for 2 minutes.

16. Clean the particles thrice using MQ water and separate between in cleaning using permanent magnet and 2 minutes.
17. Redisperse the particles in 12 mL MQ water.

A.2 Silanization of CIONPs using Batch Set-Up

1. Clean a glass vial and a magnetic stirrer bar with the solvent that will be used in the experiment.
2. Place the vial on a magnetic stirrer at 580 rpm.
3. Add 19 mL of solvent and 2 mL of TEOS to the vial and put on a lid.
4. Wait 15 minutes to ensure complete mixing.
5. Calculate the volume of CIONPs solution needed to get the desired mass of IONPs.
6. Add the CIONPs in an eppendorf tube.
7. Place the eppendorf on a permanent magnet for 2 minutes and remove the water using a glass pipette.
8. Clean the CIONPs with the solvent used in specific experiment thrice. Remove the supernatant in each step by using permanent magnet for 2 minutes.
9. Redisperse the CIONPs in 1 mL of the solvent.
10. Put the eppendorf in a ultrasonication bath for 2 minutes.
11. Pipette flush the solution in the eppendorf for 1 minute in the ultrasonication bath.
12. Add the CIONPs to the glass vial.
13. Wait 15 minutes.
14. Add the desired amount of 25wt% NH_4OH to the vial.
15. Leave the reaction mixture for 5 hours.
16. Remove the stirrer bar and transfer the solution to a centrifuge tube.
17. Place the tube next to a permanent magnet for 2 minutes and remove the supernatant.
18. Clean the particles twice with MQ water by adding 20 mL and vortex the tube. Place it next to a permanent magnet for 2 minutes and remove the supernatant.
19. Repeat the cleaning step twice using the solvent.
20. Repeat the cleaning step five times using MQ water yet again.
21. Redisperse the particles in 25 mL MQ water.

A.3 Silanization of CIONPs using a Semi-Batch Set-Up

1. Clean a glass vial and a magnetic stirrer bar with the solvent that will be used in the experiment.
2. Place the vial on a magnetic stirrer at 580 rpm.
3. Add 18 mL of solvent to the vial and put on a lid.
4. Calculate the volume of CIONPs solution needed to get the desired mass of IONPs.
5. Add the CIONPs in an eppendorf tube.
6. Place the eppendorf on a permanent magnet for 2 minutes and remove the water using a glass pipette.
7. Clean the CIONPs with the solvent used in specific experiment thrice. Remove the supernatant in each step by using permanent magnet for 2 minutes.
8. Redisperse the CIONPs in 1 mL of the solvent.
9. Put the eppendorf in a ultrasonication bath for 2 minutes.
10. Pipette flush the solution in the eppendorf for 1 minute in the ultrasonication bath.
11. Add the CIONPs to the glass vial.
12. Wait 15 minutes to ensure complete mixing.
13. Fill a syringe with the desired volume of 25wt% NH_4OH and put the syringe in a syringe pump.
14. Mix 2 mL TEOS with 1 mL solvent.
15. Fill the TEOS mixture in a syringe and put the syringe in a syringe pump.
16. Connect the syringes with NH_4OH and TEOS mixture to the vial using tubes.
17. Start pumping using the desired flow rate for NH_4OH and TEOS mixture.
18. Leave the reaction mixture for 5 hours from the moment the pumps are turned on.
19. Remove the stirrer bar and transfer the solution to a centrifuge tube.
20. Place the tube next to a permanent magnet for 2 minutes and remove the supernatant.
21. Clean the particles twice with MQ water by adding 20 mL and vortex the tube. Place it next to a permanent magnet for 2 minutes and remove the supernatant.
22. Repeat the cleaning step twice using the solvent.
23. Repeat the cleaning step five times using MQ water yet again.
24. Redisperse the particles in 25 mL MQ water.

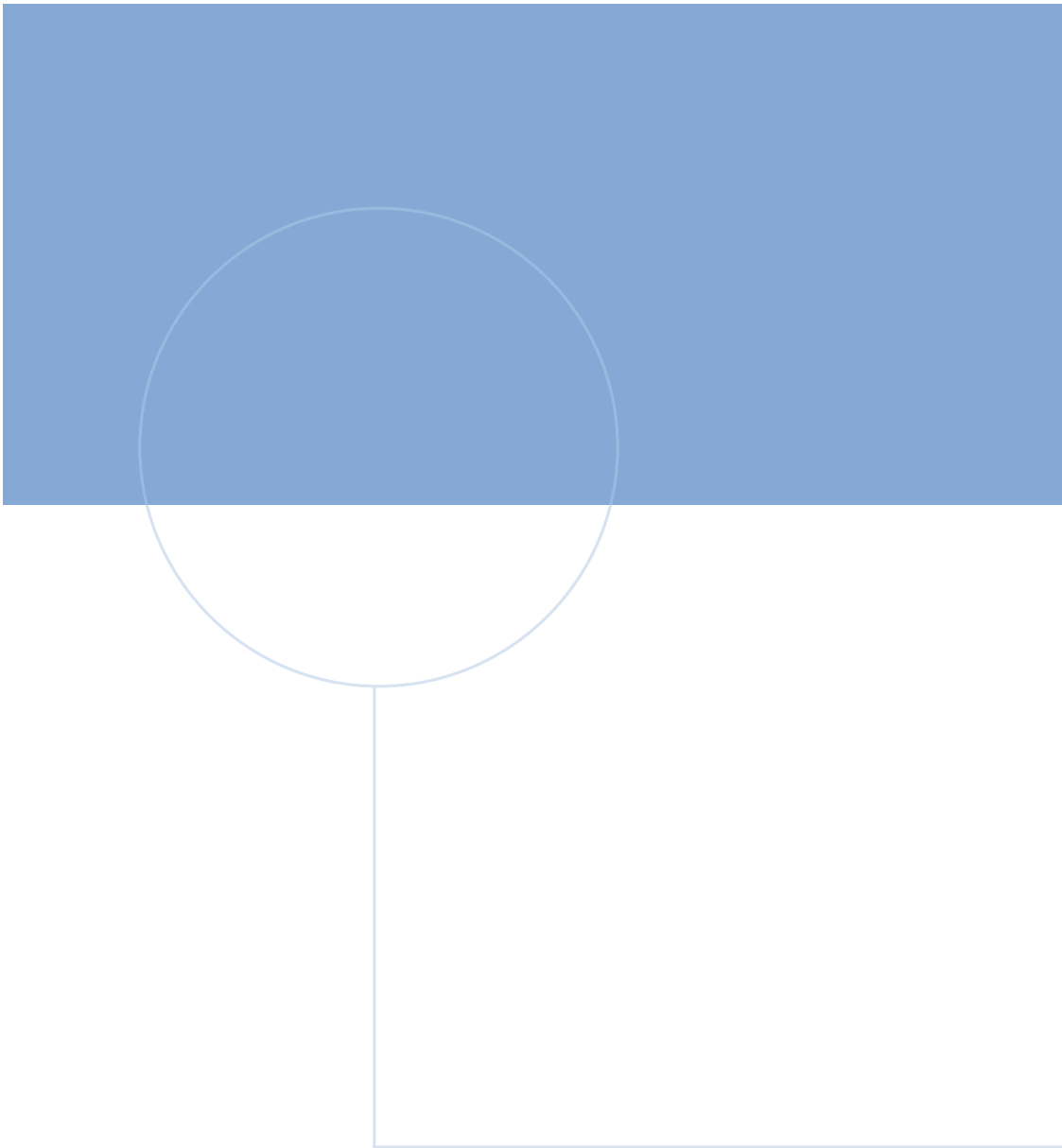

NTNU

Norwegian University of
Science and Technology